

# Motivation and challenge to capture both large scale and local transport in next generation accretion theory

ERIC G. BLACKMAN<sup>1,2†</sup> FARRUKH NAUMAN<sup>1</sup>

<sup>1</sup>Department of Physics and Astronomy, University of Rochester, Rochester, NY, 14627, USA

<sup>2</sup>School of Natural Sciences, Institute for Advanced Study, Einstein Drive, Princeton NJ, 08540, USA

(Received ?; revised ?; accepted ?. - To be entered by editorial office)

Accretion disc theory is less developed than stellar evolution theory although a similarly mature phenomenological picture is ultimately desired. While the interplay of theory and numerical simulations has amplified community awareness of the role of magnetic fields in angular momentum transport, there remains a long term challenge to incorporate insight gained from simulations back into improving practical models for comparison with observations. What has been learned from simulations that can lead to improvements beyond SS73 in practical models? Here we emphasize the need to incorporate the role of non-local transport more precisely. To show where large scale transport would fit into the theoretical framework and how it is currently missing, we review why the wonderfully practical approach of Shakura-Sunyaev (1973,SS73) is necessarily a mean field theory, and one which does not include large scale transport. Observations of coronae and jets combined with the interpretation of results even from shearing box simulations of the magnetorotational instability (MRI) suggest that a significant fraction of disc transport is indeed non-local. We show that the Maxwell stresses in saturation are dominated by large scale contributions and the physics of MRI transport is not fully captured by a viscosity. We also clarify the standard physical interpretation of the MRI as it applies to shearing boxes. Computational limitations have so far focused most attention toward local simulations but the next generation of global simulations should help to inform improved mean field theories. Mean field accretion theory and mean field dynamo theory should in fact be unified into a single theory that predicts the time evolution of spectra and luminosity from separate disc, corona, and outflow contributions. Finally, we note that any mean field theory, including that of SS73, has a finite predictive precision that needs to be quantified when comparing the predictions to observations.

**PACS codes:** Authors should not enter PACS codes directly on the manuscript, as these must be chosen during the online submission process and will then be added during the typesetting process (see <http://www.aip.org/pacs/> for the full list of PACS codes)

---

## 1. Introduction

Building on earlier notions of Swedenborg (1734), Kant (1755) (and independently Laplace (1796)) proposed that the the sun and stars must have formed from material initially rotating and subject to the influence of gravity. Early scenarios could not explain

† IBM-Einstein Fellow; Simons Fellow; Email address for correspondence: blackman@ias.edu

the distribution of angular momentum in the solar system but collectively represented a step toward accretion disc theory. Two additional paths toward modern accretion theory emerged in the 20th century from (1) the context of stars accreting from an ambient medium (Hoyle & Lyttleton 1939; Bondi 1952) and (2) from a need to explain the extraordinary compact powers of quasars and extragalactic radio sources. The latter observations stimulated explication of how the release of copious positive kinetic or radiative energy can occur as dense material falls deeper into a negative energy gravitational potential well (Shklovskii 1963; Salpeter 1964; Zel'dovich 1964).

The importance of angular momentum transport (and thus discs) in this process, and the development of specific hydrodynamic models for close binary systems (Prendergast & Burbidge 1968) along with magnetohydrodynamic (MHD) scenarios for quasars (Lynden-Bell 1969) soon emerged. Shortly thereafter, proteges of Zeldovich developed the now famous 1-D axisymmetric  $\alpha$  disc formalism (Shakura & Sunyaev 1973) connecting accretion dynamics to observed spectra. This formalism has provided the most commonly used practical framework for comparing predicted accretion disc continuum spectra to observations for accretion engines of all scales.

Essential for understanding accretion discs is determining how material can lose enough angular momentum to fall deeper into the potential well and sustain the output power. This need for angular momentum transport arises because material that becomes an accretion engine typically originates from radii many orders of magnitude away. If angular momentum is conserved upon infall, the ratio of orbital speed to Keplerian speed varies as the square root of the distance to the central engine. Therefore, material can fall in conserving angular momentum only down to the radius at which the local Keplerian speed is reached. Inside of this radius, further infall requires a loss of angular momentum.

The time scale for angular momentum loss determines the accretion time scale. When observed time scales from variability and/or system lifetimes are combined with independent estimates of disc surface densities, estimates of the efficacy of angular momentum transport can be made. Dwarf novae (DN) provide the most demanding constraints (King *et al.* 2007; Kotko & Lasota 2012). Commensurate with constraints from active galactic nuclei (AGN) and young stellar objects (YSOs), they demand that the angular momentum transport rate exceed, by many orders of magnitude, that which microphysical transport can provide. In recent decades, an amusing irony has also emerged however: all galaxies likely harbor central black holes but only a small fraction have active engines. Most are under-active, being either radiatively inefficient accreters or are being fueled with very low accretion rates. (See Yuan & Narayan (2014) for a review of radiatively inefficient accretion modes.) The need for mechanisms that lead to enhanced angular momentum transport in luminous sources is thus complemented by the need for unusual quiescence in others, or temporally evolving states within the same source. Microquasars highlight the dramatic quasi-cyclical temporal evolution within single sources (Kylafis & Belloni 2015), and possibly also provide scaled down analogues for the temporal evolution of AGN. In short, all of this highlights that we do not have as textured an understanding of the evolution of accretion engines as we do of stars.

Note also that despite the theoretical likelihood, observations supporting the universality of specifically disc accretion are mostly indirect, coming from observed spectra and luminosity considerations. Perhaps the best evidence in AGN comes from spectral analysis of the relativistic iron line profiles in Seyferts and their agreement in numerous cases with simple relativistic flat disc models illuminated from above by coronae (Risaliti *et al.* 2013; Reynolds 2014), although there remain some uncertainties with respect to how the reprocessing and X-ray illuminating material is configured, the interplay between continuum changes and line changes, and the associated atomic physics. In YSOs,

discs are observed directly (Stapelfeldt *et al.* 2014) but most of their emission comes in the infrared from dust-reflected stellar light, not accretion itself (Calvet *et al.* 2005; Kim *et al.* 2013).

Mechanisms of enhanced angular momentum transport in discs can be divided into two categories: large scale (non-local) and small scale (local) transport. Large scale transport is an appropriate characterization when the stress that transports the angular momentum is dominated by structures comparable to or larger than macroscopic disc thicknesses. Cases of predominantly large scale transport include those dependent on large scale magnetically mediated outflows Blandford & Payne (1982); Königl (1989) or large scale magnetic loops Lynden-Bell (1969). Small scale transport is the appropriate characterization when the structures dominating transport have spatial scales smaller than the disc scale height. The concept that transport can be modeled by a turbulent viscosity (Salpeter (1964); Shakura & Sunyaev (1973)) is more justifiable from first principles when small scale rather than large scale structures dominate the transport. The formalism is often used as a simplifying proxy even when the physical distinction between large and small scale transport is not made.

Because of the practicality of the axisymmetric transport model of Shakura & Sunyaev (1973) (hereafter SS73), in which the combination of Reynolds and Maxwell radial stresses are replaced by a term proportional to a "turbulent viscosity", much research has followed in an effort to identify instabilities to drive the turbulence that might produce this "viscosity." A leading candidate, and conceptual breakthrough, has resulted from application of the magnetorotational instability (MRI) (Velikhov 1959) to accretion discs (Balbus & Hawley 1991, 1998). The key insight from the latter was that in the context of Keplerian accretion discs, the linear instability criterion for the MRI requires only a radially decreasing angular velocity. In contrast, the hydrodynamic analogue that requires a radially decreasing angular momentum gradient. An accretion disc is thus linearly unstable to the former but stable to the latter.

But after decades later of substantial and important numerical simulation work on the MRI, there remains a significant gap between the output of simulations and incorporating them into a next generation, practical theory of accretion beyond SS73 for use by modelers. (A somewhat analogous circumstance is the relation between mixing length theory of convection to that of the extensive numerical simulations of convection.) In this paper, we highlight the need to close this gap. This includes synthesizing recent numerical results showing that transport from the MRI is not consistent with a small scale viscosity. In section 2 we discuss how accretion theory is normally used in model building, what is missing, and how standard SS73 accretion theory emerges from a formal mean field theory that does not include large scale transport. We also discuss the importance of quantifying the precision of mean field theories. In section 3 we discuss lessons about large scale transport from the observational interpretation of jets and coronae. In section 4 we discuss various pieces of evidence for large scale transport even from shearing box simulations. There we also revisit the physical interpretation of the MRI applicable to a shearing box. In section 5 we discuss specific open questions for shearing box studies, and in 6 we discuss more fundamental open challenges for understanding the role of large scale magnetic fields. We conclude in section 7.

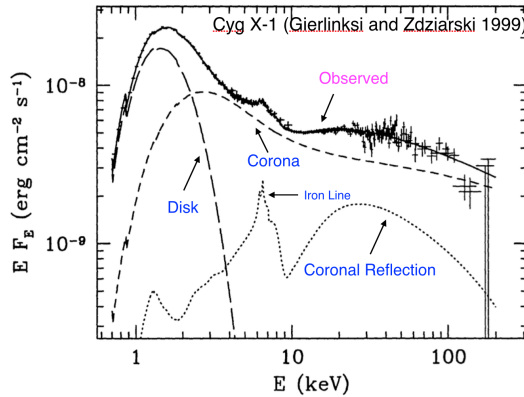


FIGURE 1. Cyg X-1 flux spectrum as an example of how engine models are patched together to match observations. Typically the optically thick continuum contribution to the disc spectrum is computed from an SS73 type model while the optically thin coronal spectrum is separately computed from a hot optically thin inverse-Compton dominated plasma. The two are then added in the relative combination needed to match the observations. The reflected spectrum is self-consistently computed given the coronal spectrum and assumptions about the disc geometry. What is missing is a self-consistent theory that predicts, from first principles, the relative contribution of disc, corona, and jet without having to patch together separate spectra empirically.

## 2. Standard Accretion Theory is a Mean Field Theory Based on Local Angular Momentum Transport

### 2.1. How Standard Disc Theory is Used

The ultimate goal of accretion theory is to explain and predict observations of accretes, most fundamentally, the observed flux, radiation spectra, and temporal evolution. Accretion engines include not only emission from the disc but contributions from large scale outflows, extended coronae, or reprocessed emission from the central star as in the case of YSOs Calvet *et al.* (2005). The ionization complexity, the mixture of material in different states of matter, and the potential role of self-gravity make YSO accretion discs possibly the most challenging. A separate set of complexities for black hole accreting disc includes the effects of radiation pressure, general relativity for the most rapid rotators, and the associated fact that outflows can be powered by magnetically mediated extraction of the rotational energy of the black hole. The latter is a separate energy reservoir from that of the accretion, although the latter would supply the magnetic field.

But even for an accretor without an additional energy source from a spinning central gravitater, the accretion itself can be a source of an optically thick disc, optically thin corona, and outflows. Presently, modelers commonly construct spectral models by pasting together empirically weighted contributions from these ingredients at the fractions needed to match observations. Fig 1 shows this for Cygnus X-1, a well known X-ray microquasar (Gierliński & Zdziarski 1999). The three contributions needed to match the spectrum are the continuum optically thick disc emission, direct optically thin coronal emission, and disc-reprocessed coronal emission. The reprocessed coronal emission is determined self-consistently, but the relative fractions of direct coronal and disc emission are tuned to match the observations. A more developed theory of accretion discs would avoid this empirical tuning. That is, given the engine size (and perhaps spin) parameters along with the accretion rate, a developed theory of accretion would allow us to directly predict the relative contributions of the emitting components from and thus the overall spectra from

first principles. We would ultimately like such a theory to also predict the time evolution of these relative fractions as the accretion rate evolves.

## 2.2. Standard Disc Theory Does not Distinguish Local vs. Non-Local Transport

The standard SS73 “viscosity” formalism is elegantly suited for capturing the local radial transport of angular momentum within the disc, but the inclusion of non-local and vertical transport requires further developments. Among the important legacies of SS73 is thus the opportunity for further work to build a more inclusive, but still practical framework.

To explain this further we emphasize that the SS73 formalism makes sense only as a mean field theory. This follows because all dynamical quantities such as velocity and density are taken to be axisymmetric, and thus a function only of radius. But if angular momentum is transported by a turbulent viscosity, axisymmetry cannot apply on arbitrarily small scales. Thus the equations for standard disc theory must emerge from mean field equations. To derive the theory, dynamical quantities such as velocity, magnetic field, density, and pressure must be divided into mean and “fluctuating” quantities, with suitably chosen averages of the latter vanishing. While this procedure is not formally shown in SS73, a first principles approach using with different averaging procedures (Balbus & Hawley (1998); Kuncic & Bicknell (2004)) reveals that the turbulent viscosity emerges from a specific closure approximation to the correlated stresses associated with magnetic and velocity fluctuations.

To see more explicitly the origin of turbulent viscosity and the limitations, note that the rate of change of vertical angular momentum for a magnetohydrodynamic disc can be obtained by multiplying the azimuthal  $\phi$  component of momentum density by radius in cylindrical coordinates. This gives (Balbus & Hawley 1998)

$$\partial_t(\rho r v_\phi) + \nabla \cdot \left[ r \rho v_\phi \mathbf{v} - r \frac{\mathbf{B} B_\phi}{4\pi} + r \left( P_{th} + \frac{B_r^2 + B_z^2}{8\pi} \right) \hat{\mathbf{e}}_\phi \right] - \nabla \cdot \left[ \frac{r \nu_V \hat{\mathbf{e}}_\phi \nabla \cdot \mathbf{v} + r^2 \nu_V \nabla \frac{v_\phi}{r} \right] = 0, \quad (2.1)$$

where  $\rho$  is the density,  $P_{th}$  is the thermal pressure,  $r$  is the radius,  $\mathbf{B} = (B_r, B_\phi, B_z)$  is the magnetic field,  $\mathbf{v} = (v_r, v_\phi, v_z)$  is the velocity,  $\nu_V$  is the dynamic viscosity, and  $\hat{\mathbf{e}}_\phi$  is a unit vector in the  $\phi$  direction. We assume radiation pressure is subdominant.

The sum of the square bracketed quantities is the total angular momentum flux. We are interested in the transport of angular momentum radially and vertically but not azimuthally. Since the divergence of  $\hat{\mathbf{e}}_\phi$  zero, any terms multiplying  $\hat{\mathbf{e}}_\phi$  (including the contributions to the second and third terms from the  $\phi$  vector components) make no contribution to the radial or vertical fluxes. The terms proportional to  $\nu_V$  are microphysical dissipation terms and we assume here that they are negligible for high Reynolds number and magnetic Reynolds number astrophysical contexts. Removing the  $\phi$  terms and the microscopic flux terms leaves the vertical and radial fluxes associated with macroscopic flows, namely

$$F_z = r \rho [v_\phi v_z - v_{Az} v_{A\phi}] \quad (2.2)$$

and

$$F_r = r \rho [v_\phi v_r - v_{Ar} v_{A\phi}], \quad (2.3)$$

where we have defined the Alfvén speed as  $\mathbf{v}_A = (v_{Ar}, v_{A\phi}, v_{Az}) = \left( \frac{B_r}{\sqrt{4\pi\rho}}, \frac{B_\phi}{\sqrt{4\pi\rho}}, \frac{B_z}{\sqrt{4\pi\rho}} \right)$ . So far, all quantities can depend on  $r, \phi, z$  and it is only after a formal averaging that we obtain a reduction of independent variables. Different procedures involving some combination of ensemble, temporal, or spatial averages can be used. For compressible flows, a convenient approach is to use density-weighted time-averages and density-weighted az-

imuthal averages (Kuncic & Bicknell 2004). Averages of density are taken to be time and azimuthally averaged so that splitting  $\rho$  into mean and fluctuating components gives

$$\rho = \bar{\rho} + \rho', \quad (2.4)$$

where  $\langle \rho' \rangle = \bar{\rho}' = 0$  and  $\langle \rho \rangle = \bar{\rho} = \frac{\int_0^{t_M} \int \rho(r, \phi, z, t+t') d\phi dt'}{2\pi t_M}$ , where  $t_M$  is a long time scale compared to turbulent turnover time scales. Averages of velocities, Alfvén speeds and their higher order moments, are taken to be *density-weighted* azimuthal and time-averages and indicated by a "tilde". For example, for the velocity we have

$$\tilde{\mathbf{v}} \equiv \langle \mathbf{v} \rangle = \frac{\int_0^T \int \rho(r, \phi, z, t+t') \mathbf{v}(r, \phi, z, t+t') d\phi dt'}{2\pi T \bar{\rho}} \quad (2.5)$$

with the assumption that the density and velocity fluctuations are uncorrelated, i.e.  $\langle \rho' \mathbf{v}' \rangle = 0$ . For the combination of density and two velocities for example, this averaging procedure then gives

$$\langle \rho v_r v_z \rangle = \bar{\rho} \tilde{v}_r \tilde{v}_z + \bar{\rho} \langle v'_r v'_z \rangle, \quad (2.6)$$

where we have made the additional approximation that triple correlations vanish to obtain the last term. Then  $\langle \rho v'_r v'_z \rangle = \bar{\rho} \langle v'_r v'_z \rangle$  after using Eq. (2.4).

Applying the above averaging procedure to Eqs. (2.2) and (2.3) gives

$$\langle F_z \rangle = r \bar{\rho} [\tilde{v}_\phi \tilde{v}_z - \tilde{v}_{A\phi} \tilde{v}_{Az} + \langle v'_\phi v'_z \rangle - \langle v'_{A\phi} v'_{Az} \rangle] \quad (2.7)$$

and

$$\langle F_r \rangle = r \bar{\rho} [\tilde{v}_\phi \tilde{v}_r - \tilde{v}_{A\phi} \tilde{v}_{Ar} + \langle v'_\phi v'_r \rangle - \langle v'_{A\phi} v'_{Ar} \rangle]. \quad (2.8)$$

These mean fluxes are functions of  $r$ ,  $z$ , and coarse grained in  $t$ .

To further simplify without completely eliminating the  $z$  dependence, we integrate separately over hemispheres. This additional coarse graining is indicated by the subscript " $\bar{\rho}$ ". Thus  $\langle \tilde{v}_z \rangle_{\bar{\rho}} \equiv \frac{\int_0^{H/2} \bar{\rho} \tilde{v}_z dz}{\Sigma/2}$ , where  $\Sigma/2 = \int_0^{H/2} \bar{\rho} dz$  and  $H$  is the disc thickness defined by a density scale height. We also assume that the three quantities  $\tilde{v}_\phi$ ,  $\tilde{v}_r$ , and  $\tilde{v}_{A\phi}$  are independent of  $z$ . The results of the  $z$  integration of Eqs. (2.7) and (2.8) are then

$$\langle F_z \rangle_{\pm} = \frac{\Sigma r}{2} [\tilde{v}_\phi \tilde{v}_{z\pm, \bar{\rho}} - \tilde{v}_{A\phi} \tilde{v}_{Az\pm, \bar{\rho}} + \langle v'_\phi v'_z \rangle_{\pm, \bar{\rho}} - \langle v'_{A\phi} v'_{Az\pm, \bar{\rho}} \rangle_{\pm, \bar{\rho}}] \quad (2.9)$$

and

$$\langle F_r \rangle_{\pm} = \frac{\Sigma r}{2} [\tilde{v}_\phi \tilde{v}_r - \tilde{v}_{A\phi} \tilde{v}_{Ar\pm, \bar{\rho}} + \langle v'_\phi v'_r \rangle_{\pm, \bar{\rho}} - \langle v'_{Ar} v'_{A\phi} \rangle_{\pm, \bar{\rho}}], \quad (2.10)$$

where the  $\pm$  subscripts indicate the values in the "+" (upper) and "-" (lower) hemispheres, but there is otherwise no  $z$  dependence left. In each hemisphere, the quantities remain functions of radius and coarse grained time. The stresses presented in this form offer a unifying focal point for a variety of generalizations of SS73, and keeping the hemispheres averaged separately is relevant for tracking any pseudo scalars (such as helicities) or fluxes into coronae that might play a dynamical role.

To see SS73 emerge from these equations, we take  $\tilde{v}_z = \tilde{v}_{Az} = \tilde{v}_{Ar} = 0$ , and ignore vertical stresses from fluctuations. Then, only the radial flux from Eq. (2.9) matters. If we further assume the  $\pm$  contributions are equal (symmetric across the mid plane) then

$$\langle F_r \rangle = \langle F_r \rangle_+ + \langle F_r \rangle_- = \Sigma r [\tilde{v}_\phi \tilde{v}_r + T_{r\phi}], \quad (2.11)$$

where  $T_{r\phi}$  is now the stress combination from fluctuations given by

$$T_{r\phi} = \langle v'_r v'_\phi \rangle - \langle v'_{Ar} v'_{A\phi} \rangle \simeq -\nu_T r \partial_r \Omega \sim q \alpha_{ss} c_s^2, \quad (2.12)$$

where the penultimate similarity (Lynden-Bell & Pringle 1974) represents the closure that converts a sum of second order fluctuation correlations into a term linear in the angular velocity shear. The latter similarity follows from setting  $\nu_T \equiv \alpha_{ss} c_s H$ , where  $\alpha_{ss}$  is the dimensionless SS73 “viscosity” coefficient, along with  $\Omega \simeq c_s/H$  in hydrostatic equilibrium, and  $\Omega \propto r^{-q}$ , where  $q = 3/2$  for Keplerian flow. Although SS73 warned that  $\alpha_{ss}$  could be a function of radius, it has become common practice to employ the simplest model in which  $\alpha_{ss}$  is a constant.

We can now recover a standard form of the accretion rate balance equation in the steady-state. Applying Gauss’ theorem to Eq. (2.1) in cylindrical coordinates with only a radial derivative and integrating the flux divergence when vertical stresses are ignored, implies that  $r\langle F_r \rangle$  is constant. If we further assume that stresses from fluctuations vanish at the inner boundary  $r = r_0$ , then using  $r\langle F_r \rangle|_{r=r_0} = r\langle F_r \rangle$  in Eq. (2.11) along with  $\dot{M} = -2\pi\Sigma r\tilde{v}_r$  for the steady-state accretion rate, we obtain

$$-\frac{\dot{M}r_0^2\Omega_0}{2\pi} = -\frac{\dot{M}r^2\Omega}{2\pi} + r^2\Sigma T_{r\phi}. \quad (2.13)$$

Thus

$$T_{r\phi} = \frac{\dot{M}\Omega}{2\pi\Sigma} \left( 1 - \frac{r_0^{2-q}}{r^{2-q}} \right) \quad (2.14)$$

for  $\tilde{v}_\phi = \Omega r$ , and  $\Omega = \Omega_0(r/r_0)^{-q}$ . A positive stress implies positive accretion for  $q < 2$ . For  $q > 2$ , this equation alone would suggest excretion but for this regime epicyclic frequencies become imaginary and the orbits and disc are unstable, violating the validity of the steady-state assumed above, and invalidating the excretion interpretation. This is also why the shearing box model produces runaway mean velocities for  $q > 2$  and is unsuitable for that regime (Nauman & Blackman 2014).

The above derivation highlights that a physically consistent derivation of the standard  $\alpha_{ss}$  viscous disc accretion model from the MHD equations requires the following: (i) formal averaging that leaves the mean field quantities dependent only on radius; (ii) dropping vertical transport terms associated with large scale fields; (iii) dropping vertical transport terms associated small scale MHD fluctuations; (iv) dropping radial transport terms associated with large scale magnetic fields; (v) including the radial transport from fluctuations by replacing the sum of their stress contributions by a viscous term linear in the mean angular velocity gradient. There is a significant opportunity to improve this standard theory by relaxing even one of the above assumptions. The importance of large scale fields, as evidenced by jets or coronae, often invalidates assumption at least assumption (ii) above. In addition, vertical stresses associated with fluctuations can be smaller than the radial stresses by a factor  $H/r$  but still contribute equally to the torque when both radial and vertical torques are present, violating assumption (iii). Radial transport by large scale loops is excluded by assumption (iv), which may also be a significant restriction (see also Rüdiger (1987)). Note that even if stresses from large scale structures might be written as proportional to  $c_s^2$  by analogy to that of viscous transport, the dimensionless coefficient can be different for that contribution, corresponding to large scale structures which fuel coronae and outflows compared to local viscous transport which supplies heating within the disc.

The standard SS73 closure modeling the transport as purely viscous is a simple and elegant, but there have been early hints that it may be misleading when applied to MRI driven turbulence (Balbus & Hawley 1998). There have been specific attempts to improve the closure (Ogilvie 2003; Pessah *et al.* 2006), and more recent direct evidence that the MRI stress does not agree with the SS73 formulation (Pessah *et al.* 2008; Nauman &

Blackman 2015). As discussed further below, our interpretation of numerical evidence further suggests that the transport from the MRI is actually dominated by large scales.

How does previous work on accretion disc theory connect to relaxing assumptions ( $i - v$ )? Blandford & Payne (1982) and Königl (1989) exemplify models for which the primary angular momentum transport occurs via large scale magnetic fields. Such models implicitly include ( $i$ ), ( $ii$ ) and ( $iv$ ), but not ( $iii$ ) and ( $v$ ). Blandford & Begelman (1999) and Quataert & Narayan (1999) are examples of practical models which include mass loss to reduce disc luminosity, and thus implicitly the role of vertical transport, but the associated stresses are not formally derived from a closure nor are the outflows emergent from equations that include large scale magnetic field dynamics. The models are rooted in the viscous formalism of assumption ( $v$ ) with the additional assumption that in collisionless plasmas, the dissipation can may heat primarily ions not electrons, and the coupling of the two being limited primarily by Coulomb collisions. Understanding the physics of this dissipation (Blackman 1999) and energy transfer is itself an important area of active research at the small scale, collisionless frontier of accretion theory (Quataert *et al.* 2014), but is outside of the scope of the present paper.

Rüdiger *et al.* (1993); Campbell & Caunt (1999); Campbell (2000) developed models for accretion that transfer angular momentum via large scale  $\alpha - \Omega$  dynamo-produced fields, and showed that this contribution to transport can be comparable to that from turbulent transport of the SS73 type. Campbell (2003) solved for the vertical structure and radial structure in such discs. Taken together, these papers maintain assumption  $v$  above but relax the others. They should be revisited with an eye toward reducing the complexity and to incorporate new developments from large scale dynamo theory (see sections 4.2 and 4.3). A separate important step towards a first principles improvement to mean field disc theory is Kuncic & Bicknell (2007) which adopts  $i$ ,  $ii$  and  $iv$  and  $v$  but drops  $iii$  by including some vertical transport. Campbell & Caunt (1999); Campbell (2000, 2003) did not compute the observed spectral influence of the vertical transport and Kuncic & Bicknell (2004, 2007) partially did but only by removing it from the contribution to the disc spectra. Overall, there remains much opportunity for further work.

### 2.3. Averaging and Precision of Disc Theory

That standard  $\alpha_{ss}$  accretion disc theory is a mean field theory means that the precision of the predictive power is limited in spatial, temporal, and spectral resolution. Without quantifying this precision and recognizing that it is finite, a disagreement between theory and observed data can be misinterpreted to imply the need for new physics rather a consequence of statistical fluctuations within the predicted precision error.

To obtain to the standard link between accretion and stress in the previous section, we considered a time-average and a  $z$ -integration without averaging in  $r$ . The longer the duration over which the time-average is taken, the lower the predicted error in precision. In comparing theory with data, it is important to know the time scales over which the data are binned to be sure that appropriate theoretical averages are being used to compare to with appropriately averaged data. The smaller the scales of turbulent fluctuations compared to the smoothing scales, the more agreement (and thus freedom in choice) there is between temporal, ensemble, and quasi-local spatial averages. However, if fluctuations are sufficiently large, then there may be a mismatch between predictions of the theory and observations taken over very short integration times even if the theory would correctly explain the data averaged over much longer times. The case of YSOs is particularly noteworthy because data against which theory is often compared are integrated for time scales much smaller than an orbit time. Some work on this mismatch



between the statistically expected deviations from the predicted mean field theory has been done (Blackman 1998; Blackman *et al.* 2010) but more is needed to address the non-local contribution of emission to a given wavelength.

A related subtlety is that although variability and deviations from standard predictions of axisymmetric theory may arise from systematic phenomena such as warps (Hartnoll & Blackman 2000; Tremaine & Davis 2014), when the theory itself uses a viscous model for transport, self-consistency requires an assessment that the predicted structures are large compared to scales of the statistical fluctuations over which the mean field theory is averaged.

#### 2.4. Local Radial Transport is Insufficient: Vertical and Nonlocal Transport Must be Included

Although most accretion disc modeling presumes a viscosity transport model and a constant  $\alpha_{ss}$ , observations and simulations challenge this minimalist paradigm. Evidence for its insufficiency emerges from: (1) observations indicating non-local radial and vertical transport via jets, outflows, and coronae and the important role of large scale fields in plausible jet models. (2) inadequacy of total stress magnitudes derived from local shearing box MRI simulations if taken at face value; (3) dominance of large scale stresses in local and global simulations; (4) contradiction between transport computed from simulations and the dependence on shear predicted from the constant  $\alpha_{ss}$  viscosity model. (5) evidence that  $\alpha_{ss}$  depends on radius in some global simulations Penna *et al.* (2013). We discuss points 1-4 further below.

### 3. Lessons From Observations of Jets, Coronae, and Large scale structures

Jets and coronae are conspicuous components of accretion engines and highlight the importance of vertical transport. Seyfert AGN observations reveal  $\geq 30\%$  of bolometric emission coming from corona-produced X-rays (Mushotzky *et al.* 1993) and in some radio sources and blazars, jets even have more mechanical luminosity than the underlying discs alone can provide (Ghisellini *et al.* 2014) (requiring input from the central rotator). These circumstances indicate the prevalence of large scale modes of transport. In sub-Eddington sources, Large scale magnetic fields provide natural angular momentum transport agents (Blandford & Payne 1982; Königl 1989; Field & Rogers 1993; Blackman *et al.* 2001; Lynden-Bell 2006; Pudritz *et al.* 2012; Penna *et al.* 2013). In young stars, pre-planetary nebulae, microquasars, and active galactic nuclei, jets typically have too much collimated momenta to be driven by mechanisms that do not involve large scale magnetic fields (Pudritz *et al.* 2012; Blackman & Lucchini 2014). In the jets of AGN, Faraday rotation from ordered helical magnetic fields is directly observed (Taylor & Perley 1993; Asada *et al.* 2008; Gabuzda *et al.* 2012).

Magnetized outflows anchored in accretion engines can extract angular momentum without expelling much mass, allowing the remaining disc material to accrete. Jet formation may depend on role large scale fields also play in coronae: if discs are turbulent, then coronae likely emerge from disc magnetic ejecta whose structures are large enough to escape turbulent shredding on a buoyant rise time (Blackman & Pessah 2009). Once these structures arrive to the coronae, they can further open up by dynamical relaxation to form large scale fields that facilitate jets. In many objects, broader winds, in addition to jets, may also provide a loss of angular momentum. The common presence of corona, jets, and outflows raises a generic question of whether accretion may in fact *require* out-

flows. This highlights a substantial deviation from solely local radial transport of angular momentum.

Outflows and coronae can in principle be included in extensions of disc models with zero-stress internal boundaries and steady accretion, but real discs also have more varied boundary conditions that lead to additional large scale features. For example, the magnetospheric coupling between disc and stellar field has been long studied in the context of compact objects (Ghosh & Lamb 1978; Perna *et al.* 2006) and YSOs (Matt & Pudritz 2005; Romanova *et al.* 2012; Lii *et al.* 2014; Lai 2014). Large scale vortices, either hydrodynamically (Lovelace *et al.* 1999; Li *et al.* 2000; Colgate *et al.* 2003; Klahr & Bodenheimer 2003; Barranco & Marcus 2005) or magnetically induced (Tagger & Pellat 1999; Varnière & Tagger 2002), also provide modes of non-local transport. Self-gravity can also produce large scale features such as spiral arms that induce transport and encompass another set of processes (Gammie 1996; Gammie & Menou 1998; Vorobyov & Basu 2007; Zhu *et al.* 2009). In YSOs, large scale disc structures are now observed with ALMA (van der Marel *et al.* 2013; Pérez *et al.* 2014).

King *et al.* (2007); Kotko & Lasota (2012) point out that Dwarf Novae and AGN require  $0.1 \lesssim \alpha_{ss}\beta \lesssim 0.4$  in the SS73 viscous paradigm, which is a factor of 10 larger than what the "best converged" modern shearing box MRI simulations produce e.g. (Davis *et al.* 2010). Because of the limitations of the theory and the simulations, lingering questions about convergence (Bodo *et al.* 2014), and the physical applicability of what is learned from the shearing box can be debated, but the factor of 10 discrepancy may be indicative of transport occurring on much larger scales than what a shearing box is able to capture.

#### 4. Lessons from Shearing Boxes

The widely used local shearing box is a very powerful tool (Balbus & Hawley 1998) to study aspects of transport and the associated nonlinear MHD even though it fundamentally differs from a local section of a real disc. The shear periodic radial boundaries reduce the accessible phase compared to a real system and there is a symmetry between outward and inward radial directions that is broken for a real disc because the latter has a finite radius of curvature. The boxes also can lead to an injection of Poynting flux due to the non-periodicity of the azimuthal velocity (Hubbard *et al.* 2014). Shearing boxes to date also do not include vertical shear (McNally & Pessah 2014).

Since the radius of curvature is infinite for a shearing box, the angular momentum is ill-defined and there is no finite divergence of the angular momentum fluxes and thus no torque. What we learn about transport from shearing boxes comes from computing the stresses. As mentioned above, the basic question of convergence of stresses is still under debate (Davis *et al.* 2010; Bodo *et al.* 2014). Convergence of stresses is not yet achieved for global simulations (Hawley *et al.* 2011) and more subtle questions of convergence of spectral shapes have yet to be fully vetted (Nauman & Blackman 2014). Before discussing lessons about large scale transport learned from these stresses, we first discuss the MRI a bit further in the context of shearing boxes to clarify the physical interpretation of the instability therein.

##### 4.1. Understanding the MRI in shearing boxes as a transfer of linear momentum

A widely used physical explanation for the linear MRI appeals to two masses tethered by a spring separated by an initial radial displacement in a background rotation profile of outwardly increasing angular momentum (Balbus & Hawley 1998). For a weak enough spring, the inner mass loses angular momentum to the outer mass and will continue to move toward loci of lower background angular momentum, namely, inward. Comple-

mentarily, the outer mass moves toward regions of higher background angular momenta, namely outward. By considering the equations for each mass separately and taking their difference, the expression for the separation between the masses can be obtained with exponential growth being the signature of the instability. A similar approach can be used to argue that a flow with an outwardly decreasing background angular momentum gradient should be stable to the MRI. Such stability is consistent with recent generalizations Shakura & Postnov (2014).

However, because the Cartesian shearing box has an infinite radius of curvature the angular momentum is ill-defined. But the instability is still robust therein because it manifests in the linear momentum equations. The angular momentum transport is a secondary consequence that arises for a finite radius of curvature. Although these points follow simply from the known equations, the standard physical explanation of the MRI given in the previous paragraph with angular momentum commonly presented without clarification for a shearing box. To make the clarification clear, we discuss the tethered spring analogue in more detail below.

To converting apply the viscous closure Eq. (2.12) to that of a shearing box, we shift to the local Hill frame Cartesian coordinates for a disc co-rotating with local angular speed  $\Omega_0 = \Omega(r = r_0)$ , assumed to represent the range  $r_0 - x \leq r \leq r_0 + x$ , with  $x \ll r_0$ . Ignoring curvature terms, the mean  $y$ -velocity in the box equals

$$\tilde{v}_\phi - \Omega_0 r_0 = r(\Omega - \Omega_0) \simeq xr\partial_r\Omega|_{r=r_0} = -xq\Omega \quad (4.1)$$

to lowest order in  $x$  so that

$$\langle T_{r\phi} \rangle = \alpha c_s H q \Omega_0 \quad (4.2)$$

in place of Eq. (2.12). From the right side of Eq. (4.1) we see that the center line of the box  $x = 0$  represents the co-rotation radius whose mean azimuthal ( $y$ -direction) velocity vanishes.

In the absence of pressure gradients, the Hill frame equations capturing the MRI instability (Balbus 2003) in the presence of a vertical field of strength  $B_z$ , subjected to displacement  $\boldsymbol{\xi} = (x(t)e^{ikz}, y(t)e^{ikz})$  about the vertical line ( $x = 0, y = 0$ ) can be written

$$\ddot{x} - 2\Omega\dot{y} = -(K_A - T)x, \quad (4.3)$$

and

$$\ddot{y} + 2\Omega\dot{x} = -K_A y, \quad (4.4)$$

where  $T = -rd\Omega^2/dr = 2q\Omega^2$  ( $q = 3/2$  for Keplerian) is the coefficient of the tidal force per unit mass in the Hill frame;  $K_A = (k\tilde{v}_{zA})^2$ , where  $\tilde{v}_{zA}$  is the Alfvén speed associated with the vertical field; and the second terms on the left sides come from the Coriolis force. The appearance of  $K_A$  arises as a consequence of magnetic tension force because the linear fluctuation in the field  $\delta\mathbf{B}$  satisfies  $\partial_t\delta\mathbf{B} \sim ikB\delta\mathbf{v}$  from the induction equation, so that  $\delta\mathbf{B} \sim ikB\delta\mathbf{v}t \sim ikB\boldsymbol{\xi}$  upon time integrating. The curvature force appearing on the right side of the momentum equation is then  $\frac{\mathbf{B}\cdot\nabla}{4\pi\rho}\delta\mathbf{B} \sim -K_A\boldsymbol{\xi}$  with the magnetic pressure having been absorbed into the total pressure, assumed to have a vanishing gradient.

Since the  $z$  dependence dropped out of Eqs. (4.3) and (4.4), the relevant motion takes place in the  $x, y$  plane. The equations can then be interpreted to describe the evolution of the position of a small parcel of fluid at position  $\boldsymbol{\xi}$  tethered by spring to a fixed point at the origin  $x, y = 0$ . Given that  $K_A$  and  $T$  are constants, the right hand side of the above equations then represents two directional components of a spring force per unit mass with distinct spring constants  $K_A - T$  and  $K_A$  respectively. The spring constant in Eqn. (4.4) has a positive sign, such that positive displacement strengthens the force

opposing the displacement. However, if  $T > K_A$  then Eq. (4.3) would have a negative spring constant, so the associated force would exacerbate the separation of the fluid parcel from the origin as the separation increases in the  $x$  direction. When interpreted as a runaway displacement of the fluid parcel from its initial position, instability requires  $T > K_A$  and stability requires  $T \leq K_A$  as found by solving the two equations. (Note that for  $q < 0$ , the azimuthal velocity increases outward. Then  $T < 0$ , and the effective spring constant in Eq. 4.3 would be positive, implying stable oscillations.)

Eqs. (4.3) and (4.4) equation can also be adjusted to describe the displacement of two equal density fluid parcels mutually attached by a spring. To do so, we must construct two sets of equations similar to Eqs. (4.3) and (4.4), one for each of the two masses and then subtract them to get the equations of evolution of their separation. However note that while the tidal force has the same form as in the above equations, the force from the  $K_A$  terms depends on the separation between the two masses. The equations for each of the two parcels thus take the form

$$\ddot{x}_i - 2\Omega\dot{y}_i = Tx_i - K_A(x_i - x_j), \quad (4.5)$$

and

$$\ddot{y}_i + 2\Omega\dot{x}_i = -K_A(y_i - y_j), \quad (4.6)$$

where  $i = 1, j = 2$  represents the equations of motion for parcel 1 and  $i = 2, j = 1$  represents the equations for parcel 2. Subtracting the respective  $x$  and  $y$  equations for parcel 2 from those of parcel 1, and letting  $(\zeta_x, \zeta_y) = (x_1 - x_2, y_1 - y_2)$  gives

$$\ddot{\zeta}_x - 2\Omega\dot{\zeta}_y = -(2K_A - T)\zeta_x \quad (4.7)$$

and

$$\ddot{\zeta}_y + 2\Omega\dot{\zeta}_x = -2K_A\zeta_y. \quad (4.8)$$

Instability as interpreted as separation of the two connected masses requires  $T > 2K_A$ . Neither of the above explanations of the instability criteria require explicit mention of angular momentum. The instability is evident in the linear momentum equation and the stress that it produces in the shearing box limit represents a transfer of linear momentum. For a finite radius of curvature, angular momentum transport then becomes a physical consequence.

#### 4.1.1. *Laboratory experiment to test the spring-tethered masses model of the MRI?*

We suggest that existing experimental configurations set up to ultimately study the MRI using liquid metals (e.g. Ji (2011)) could in fact be useful for also setting up a tethered mass MRI analogue experiment. Two light masses tethered by a weak spring could be placed in a Taylor-Couette flow tank using even water, and their motion tracked. Their evolution would provide data for comparison with linear theory and for comparison with the results expected for a system with a central gravitational potential. Drag forces and boundary layers around the embedded masses may provide complications but such an experiment warrants further investigation as it is conceptually relevant and likely inexpensive.

### 4.2. *Stress Spectra from Shearing Boxes: The Dominance of Large Scales*

#### 4.2.1. *Stress Spectra From Fluctuations*

The simplifications and limitations of the shearing box are significant compared to real discs, but, like the triply periodic box commonly used in forced MHD turbulence studies, the shearing box should be thought of as its own well-defined computational

physics experiment. If we can understand how fields and flows evolve in such suitably chosen minimalist systems, we hopefully gain insight into key elements of real systems.

How well are the basic assumptions of the SS73 paradigm confirmed or refuted by shearing box studies? This is germane given that stress magnitudes from shearing box simulations are widely quoted as inputs for spectral models. Shearing boxes were designed with the intuition that angular momentum transport is a primarily local, radial transport phenomena. In this context we can ask (i) what scales dominate the stresses? (ii) do the radial stresses depend linearly on shear as predicted by the SS73 framework with constant  $\alpha_{ss}$ ? As we will see below, the answers are: 1) large 2) no.

We first determine the scale dependence of stresses from from stratified shearing box simulations by computing the  $k$ -dependent cumulative stress from fluctuations (Nauman & Blackman 2014). This is computed by integrating from the minimum wavenumber up to  $k$  and determining how large  $k$  must be in the integral to capture most of the stress in the box. We have used the ATHENA code and solved the vertically stratified MHD equations without explicit diffusivities, for an isothermal equation of state. The boundary conditions are shear periodic in the radial  $x$  direction, periodic in the azimuthal  $y$  and vertical  $z$  directions (with gravity thus taken to vanish at vertical boundaries). For the results shown in Fig 2, we employed a box domain size of  $4H \times 4H \times 8H$  where  $H$  is the density scale height, with a resolution of 96 zones per  $H$  and an initial plasma  $\beta$  (thermal to magnetic pressure ratio) equal to 100 everywhere and an initially toroidal mean field which decreases in strength vertically like the density.

We obtain the cumulative stresses from fluctuations as a function of wave number by first computing 2-D Fourier transforms  $f(\mathbf{k}, z) = f(k_x, k_y, z)$  of a physical quantity  $F(\mathbf{x})$  (which was either the magnetic field, off-diagonal magnetic stress, momentum density, and off-diagonal Reynolds stress) in variables  $x$  and  $y$ . For each quantity we then computed three different integrals of the quadratic norm: (i) circle average:  $|f(k, z)|^2 = \int |f(\mathbf{k}')|^2 \delta(|\mathbf{k}'| - k) d\mathbf{k}'$ , where  $|\mathbf{k}| = \sqrt{k_x^2 + k_y^2}$ , (ii) y-integrated:  $|f(k_x, z)|^2 = \int |f(\mathbf{k})|^2 dk_y$ , (iii) x-integrated  $|f(k_y, z)|^2 = \int |f(\mathbf{k})|^2 dk_x$ . To eliminate  $z$ , we then averaged the resulting 1-D spectra over  $z$  ranges specified by either "disc" or "corona" as determined by the height above which the saturated  $\beta$  is above or less than unity respectively. The cumulative stress and energy spectra then represent the integral of a given spectrum up to wave number  $k$  divided by the integral over the full range of  $k$ , that is:

$$\begin{aligned} Q_f(k) &= \frac{\int_1^k |f(k')|^2 2\pi k' dk'}{\int_1^{k_{max}} |f(k')|^2 2\pi k' dk'} \\ Q_f(k_x) &= \frac{\int_0^{k_y} |f(\mathbf{k})|^2 dk_y / \int dk_y}{\int_0^{k_{y,max}} |f(\mathbf{k})|^2 dk_y / \int dk_y} \\ Q_f(k_y) &= \frac{\int_0^{k_x} |f(\mathbf{k})|^2 dk_x / \int dk_x}{\int_0^{k_{x,max}} |f(\mathbf{k})|^2 dk_x / \int dk_x}. \end{aligned} \quad (4.9)$$

The stresses computed as above do not include contributions for which both  $k_y = 0$  and  $k_x = 0$ , though each can separately vanish. We discuss the  $k_y = k_x = 0$  contributions in subsection 4.2.2.

Fig. 2 shows that, for both coronae and disc regions, more than half of the radial and vertical stresses are accounted for by contributions from the first few wave numbers. We found that this conclusion is independent of the box size for domain sizes studied. The cumulative stresses are dominated by correlations from large scales of the box. Even though stresses are nearly constant as the box sizes and resolutions change (a necessary condition for convergence), the upper integration bound on the wave number needed to capture 50% of the cumulative stress does not increase as the box domain size increases.

This suggests that the local simulations are insufficient to capture significant large scale contributions to the transport. That in turn highlights a limitation of the shearing box; the box size cannot be increased indefinitely without having to incorporate curvature terms or vertical shear (McNally & Pessah 2014) to ensure relevance when scaled to a real system. That shearing boxes suggest non-local transport in the sense described is further supported by measurements from global simulations of energy spectra (Flock *et al.* 2012; Suzuki & Inutsuka 2014) and stress spectra (Beckwith *et al.* 2011; Sorathia *et al.* 2012; Parkin & Bicknell 2013).

While energy spectra and stresses for both disc and coroneae (respectively distinguished by plasma  $\beta$  greater than or less than unity) in cases with net flux and without explicit dissipation are dominated by large scales in both local and global simulations and the magnetic energy spectra generally do not show a turnover at large scales (Nauman & Blackman 2014), the zero net flux, unstratified simulations of (Fromang 2010) with explicit dissipation do seem to show a turnover in the magnetic and kinetic energy spectra. The wave number of the magnetic peak seems to increase with increasing magnetic Reynolds number. A concern about magnitude of stress in previous unstratified zero flux simulations however is that they did not seem to converge Pessah *et al.* (2007), although Fromang (2010) argues for convergence. Controversy still lingers over the question of convergence of the stress magnitude, even for stratified simulations (Davis *et al.* 2010; Bodo *et al.* 2014). Stress spectra, in addition the stress magnitude, should be assessed in convergence studies.

#### 4.2.2. Comparing Stresses From Mean Fields to those From Fluctuations

The analysis of the previous section does not include contributions to the stress from  $k_x = k_y = 0$  modes at fixed  $z$ . We refer to these as stresses from the mean field. Here we compare the contribution from their stresses to those from the fluctuations. As the measure of stresses and energies from mean magnetic fields we compute  $T_{M,ij}(z) = \langle B_i \rangle \langle B_j \rangle$  where the brackets indicate  $x, y$  averages, with the product being left as a function of  $z$ . We then average the product over  $z$  and orbit times  $101 < t < 220$  to obtain the total contribution  $T_{M,ij}$ . For the measure of stress from fluctuations, we first compute the contribution from the total field  $T_{ij}(z) \equiv \langle B_i B_j \rangle$ , average over  $z$  and  $101 < t < 220$  as above to obtain  $T_{ij}$ , and then subtract the total contribution from the mean fields to obtain  $T_{Fij} = T_{ij} - T_{M,ij}$ .

Using the above procedure for a  $q = 3/2$  case from a run with 32 zones/ $H$  and domain size  $H \times 2H \times 4H$  (Nauman & Blackman 2015), we find that the ratio of the stresses from the mean field to that of the total to be  $T_{M,xy}/T_{xy} \simeq 0.24$  and that the ratio of magnetic energy from the mean field that of the total to be 0.47. These indicate a significant contribution from the mean field, bolstering the overall message that large scale fields and transport are important. The simulation from which we derived this result has no extended corona and so the stress ratio likely underestimates the importance of mean fields: Fig. 3. shows that already at the base of the corona the mean stresses are dominant.

#### 4.3. More deviations from transport as viscosity in MRI sims

Simulations in shearing boxes reveal other important deviations from the traditional constant  $\alpha_{SS}$  prediction such as the dependence on the shear profile index  $q$ . Eq. (4.2) shows that the SS73 formalism combined with the assumption of constant  $\alpha$  predicts a stress linear in  $q$ . But the dependence on shear has been found to be strongly inconsistent with such a linear dependence from both unstratified (Pessah *et al.* 2008) and stratified (Abramowicz *et al.* 1996; Nauman & Blackman 2015) simulations.

In addition, stress and magnetic energy spectra are anisotropic, being elongated in the

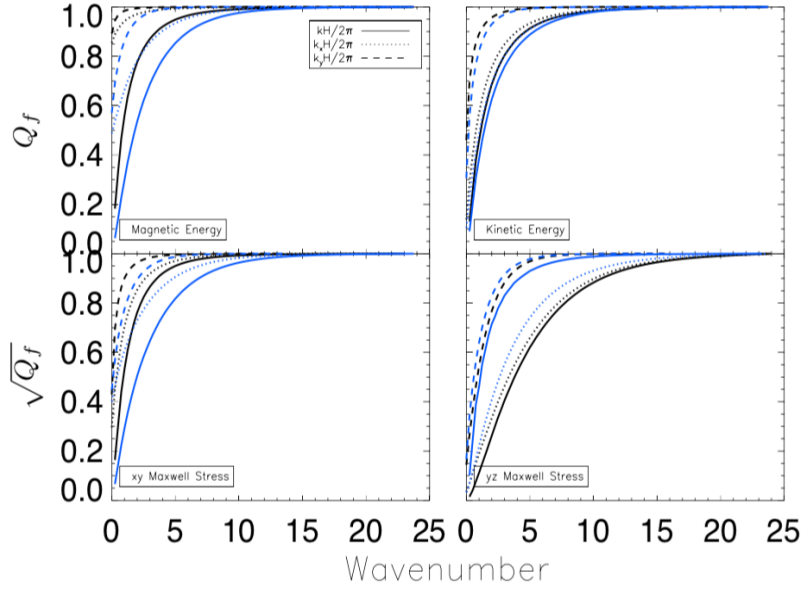


FIGURE 2. Modified from Nauman & Blackman (2014) (to include  $(0, k_y)$  and  $(k_x, 0)$  modes): the fractional spectral power for several quantities as indicated in a Keplerian shearing box simulation (see text for parameters) vs. a dimensionless measure of the wave number. Black curves are for corona  $|z| \geq 2H$  and blue curves are for disc  $|z| < 2H$  and the legend shown applies to both color sets of curves. The wave numbers are of the form  $k = 2\pi n/L$  where  $L = 4H$  is the domain size in the  $x$  or  $y$  direction and  $n$  ranges from 1 to 96. The  $x$ -axes are  $kH/2\pi = n/4$ . The total stresses are dominated by the Maxwell stresses and so lessons learned from their plots also apply for the total. Both coronae and disc show that the fractional power for all quantities is well over 50% already for the first few wave modes. Fractional power is calculated using equation 4.9 using  $|f(\mathbf{k})|^2 = \{|B(\mathbf{k})|^2, |\sqrt{\rho}v(\mathbf{k})|^2, |B_x B_y(\mathbf{k})|^2, |B_y B_z(\mathbf{k})|^2\}$  for magnetic energy, kinetic energy,  $xy$  Maxwell stress,  $yz$  Maxwell stress respectively. For energy  $Q_f$  gives the fractional power, but for the stresses it gives fractional power of stress squared, so we plotted  $\sqrt{Q_f}$  in those cases. The fractional power distribution in  $k_y$  is significantly different from that of  $k_x$  and  $k$  for all quantities, highlighting anisotropy.

$y$  direction and more so on large scales than small scales (see Fig. 2). This suggests that a nonlinear cascade ensues with turnover time scales that progressively decrease with scale compared to the shear time scale, the latter being constant on all scales.

The subtleties in anisotropy and scale dependence further highlight that stress magnitude should not be the sole criterion for convergence in MRI simulations. Convergence studies should also address the stress spectra and anisotropy. There remains opportunity for a systematic assessment of their convergence as a function of initial conditions, presence or absence of explicit dissipation, magnetic Prandtl number, resolution and local vs. global simulations.

#### 4.4. Saturation of MRI and Tilt Angle

The saturation mechanism of MRI stress in shearing boxes is still uncertain and may even differ from that of global simulations or real discs. We have emphasized that saturated stress spectra as a function of resolution and domain size should be evaluated in addition to stress magnitude as part of generalized convergence studies. However, an interesting nugget of universality (for simulations that are not radiation dominated) is a nearly constant value of  $0.1 \lesssim \alpha_{ss}\beta \lesssim 0.4$ . Blackman *et al.* (2008). Here the dimensionless

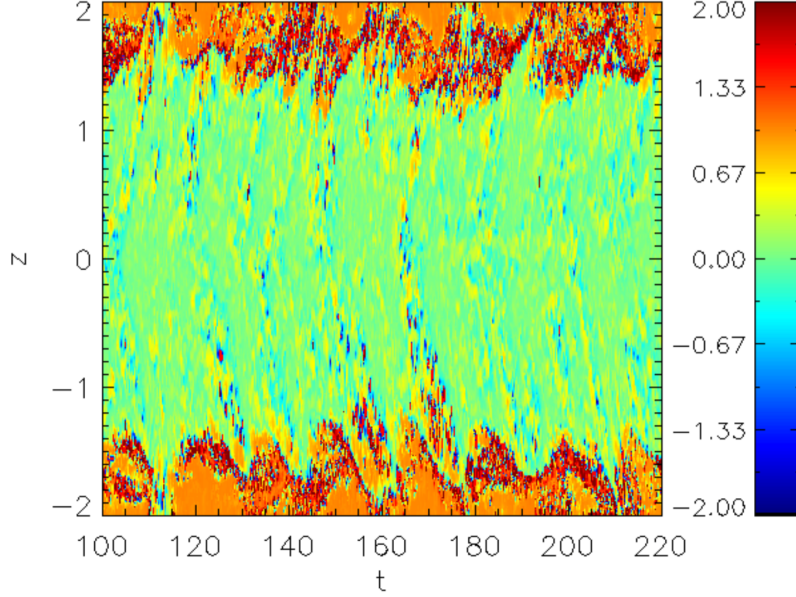


FIGURE 3. Color gradient plot the ratio of the Maxwell stress from the  $x$  and  $y$  averaged mean fields to to the  $x$  and  $y$  averaged total Maxwell stress  $T_{M,xy}(z)/T_{xy}(z)$  as a function of  $z$  and  $t$ . The data come from a vertically stratified, vertically periodic simulation of domain size  $H \times 2H \times 4H$  with 32 zones/h and shear parameter  $q = 3/2$  and initial toroidal field with initial plasma  $\beta = 100$ . The plot shows the dominance of the mean components of the stress near the top of the box. Values in excess of unity can arise because the stress is a signed quantity and the denominator  $T_{xy}(z)$  includes some non-vanishing oppositely signed contributions from cross terms between mean and fluctuations that do not vanish. This simulation has no extended corona where plasma  $\beta < 1$  but the particular importance of the large scale field where the density and saturated  $\beta$  decrease near the top of the box is evident.

measure of the stress associated with fluctuations in the SS73 formalism is  $\alpha_{ss} = \frac{T_{xy}}{P_{th}}$  and  $\beta = P_{th}/P_{mag}$ , the ratio of thermal to magnetic pressure. (For radiation dominated accreters this would be generalized to include radiation pressure and thus the constancy of  $\alpha_{ss}\beta$  might be replaced by  $\alpha_{ss}\beta_{tot}$  where  $\beta_{tot} \sim \frac{P_{rad}+P_{part}}{P_{mag}}$ .) As we show below, the near constancy of  $\alpha_{ss}\beta$  is equivalent to a constancy of the tilt angle between the azimuthal and radial fluctuating field components, and can be compared to the associated tilt angle of the mean field if planar averages are considered for the latter. Computed as box averages, stresses from mean fields would not survive in the absence of a net flux. But at a given  $z$ , mean stresses can be important, as seen in Fig 3. Below we estimate and compare the tilt angles for fluctuations and planar averaged mean fields.

#### 4.4.1. Tilt angle from fluctuating fields

Because the magnetic stress dominates the Reynolds stress we have, for the box averaged contribution from fluctuations

$$\alpha_{ss} \simeq \frac{\langle b^2 \rangle \langle b_x b_y \rangle}{P \langle b^2 \rangle} = \beta^{-1} \frac{\tan \theta}{(1 + \tan^2 \theta + b_z^2/b_x^2)} \sim \beta^{-1} \tan \theta,$$

where  $\tan \theta = b_y/b_x$ , and we assume  $|b_z/b_x| \ll 1$  and  $\tan \theta \ll 1$  for the last similarity (justified later).

The constancy of tilt angle across simulations can be explained as a consequence of the fact that the toroidal field is amplified above the radial field by shear over a time



scale approximately equal to a correlation time scale (Blackman *et al.* 2008). Roughly,  $|b_y| \sim |b_x|(1 + q\Omega\tau_c)$  implying that  $\tan\theta \sim (1 + q\Omega\tau_c)^{-1}$ . Nauman & Blackman (2015) showed that the tilt angle is also independent of the shear parameter  $q$  using ATHENA because an increase or decrease in shear is compensated by a corresponding decrease or increase in the relevant correlation time. Whether the source of the reduced correlation time is physical or a consequence of the numerical method (such as the remap time scale across the radial boundary) needs further investigation.

#### 4.4.2. Tilt angle from mean fields and comparison to that from fluctuations

Compared to that of the fluctuating fields, we expect the tilt angle from mean fields to be larger if sustained by a large scale dynamo. We explain this prediction and compare it to the data here.

In shearing box simulations, mean fields can be computed as horizontally averaged fields, left as a function of  $z$ . The large scale dynamo would, via the electromotive force, sustain the radial ( $x$ ) field whilst the azimuthal ( $y$ ) field would be stretched by shear. Although fluctuating fields can be stretched coherently on a correlation time, the mean field could be sheared coherently over the longer vertical diffusion time. For mean fields we therefore have  $\langle B_y \rangle / \langle B_x \rangle \sim q\Omega t_{df}$  where  $t_{df} = (\alpha_{ss} c_s H k_z^2)^{-1}$  is the vertical diffusion time of the mean field mode of wavenumber  $k_z$ . For  $c_s \sim \Omega H$  in hydrostatic equilibrium, we then have

$$\tan\theta_M = \langle B_x \rangle / \langle B_y \rangle \sim (\alpha_{ss}/q)(k_z H)^2 \sim \alpha_{ss}/q, \quad (4.10)$$

for  $k_z H \sim 1$ . Empirically,  $\alpha_{ss} \propto \frac{q}{2-q}$  (Abramowicz *et al.* 1996; Pessah *et al.* 2008; Nauman & Blackman 2015) so  $\tan\theta_M \simeq \frac{1.5\alpha_{ss,0}}{2-q}$ , where  $\alpha_{ss,0} \equiv \alpha_{ss}(q = 3/2)$ . Combining this latter expression with that for the fluctuating field above we predict that

$$\frac{\tan\theta_M}{\tan\theta} = \frac{1.5\alpha_{ss,0}(1 + q\Omega\tau_c)}{(2 - q)} \ll 1, \quad (4.11)$$

for  $\alpha_{ss} \sim 0.01$ . The predicted tilt angle ratio from Eq (4.11) is roughly consistent with that found in simulations: for the run shown in Fig. 3, the tilt angle for the mean field is  $\tan\theta_M = \frac{\langle B_x \rangle \langle B_y \rangle}{\langle B \rangle^2} \sim 0.03$  while the tilt angle from everything but the mean gives  $\frac{\langle B_x B_y \rangle - \langle B_x \rangle \langle B_y \rangle}{\langle B^2 \rangle} \sim 0.26$ . The ratio of these two is 0.14. The predicted ratio from Eq. (4.11) for  $\alpha_{ss,0} = 0.01$  and  $q = 3/2$  is 0.06, so not too far off. The stresses from planar averaged mean fields can be significant at given  $z$  even if the box averaged stresses appear to show tilt angles more consistent with those for fluctuations.

For large scale dynamos operating in galaxies similar questions about the tilt angle of the fluctuating and the mean fields can be considered. However, therein the turbulent diffusion is likely primarily due to supernovae and not to the MRI. Extracting the shear dependence must then include consideration of how the the turbulent diffusion does or does not correlate with the shear. That circumstance is distinct from the MRI, but useful to ponder when generally pondering predictions of large scale dynamos. Recently Van Eck *et al.* (2015) found that the shear dependence of tilt angle of the mean field in galaxies did not have a shear dependence that was easily captured by simple models.

## 5. Some Open Questions For Local Shearing Box Studies

A long term challenge is to combine insights gained from simulations into improved "textbook" mean field models that allow practical modeling of observations, but a number of open questions specifically pertinent to shearing boxes remains.

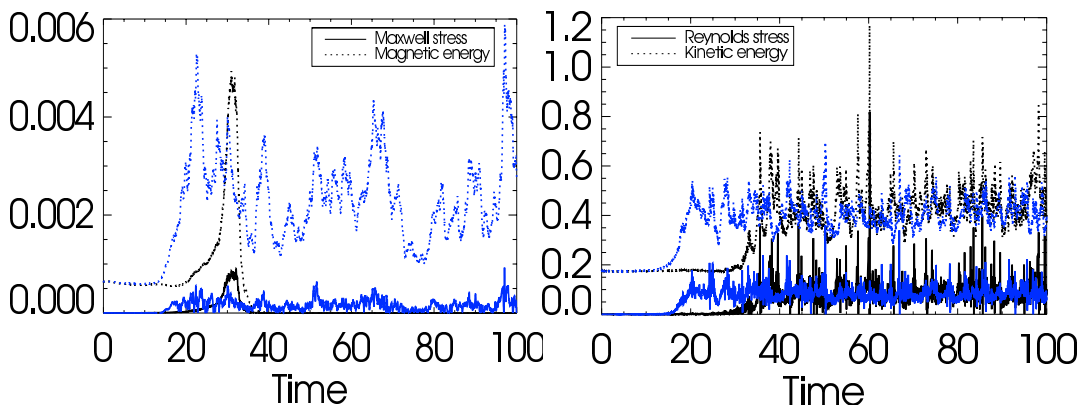


FIGURE 4. Unstratified simulations using ATHENA, showing that linear Keplerian shearing boxes without the Coriolis force are both unstable to generation of turbulence and that at high enough resolution, magnetic field is amplified. The initial conditions of the simulations were zero net magnetic flux with an initial magnetic field  $B_0 = \text{Sink}z\sqrt{2P_0/\beta}$  and an initial plasma  $\beta = P_{th}/P_{mag} = 1600$ . The domain size used in  $(x, y, z)$  is  $H \times 2\pi H \times H$ . Time units are  $2\pi/\Omega$ , with  $\Omega = 10^{-3}$ . The left panel shows the magnetic energy (dashed) and Maxwell stress (solid) and the right panel shows the kinetic energy (dashed) and the Reynolds stress (solid). In each panel the black lines are for a resolution of 16 zones/ $H$  and blue lines are for 32 zones/ $h$ . For both resolutions, the right panel shows that the kinetic energy and Reynolds stress grow. The left panel shows however, that only for higher resolution case do the magnetic energy and Maxwell stress grow. Previous simulations (Hawley *et al.* 1996) did not use high enough resolution to obtain field growth.

### 5.1. Growth of magnetic field from shear-driven turbulence without Coriolis Force

In the absence of a Coriolis force, Keplerian shearing boxes are unstable to the development of flow turbulence, but the earliest simulations of this type did not show an accompanying growth of magnetic energy Hawley *et al.* (1996). This highlighted the fact that the mere existence of turbulence does not guarantee field growth, but reason for this absence of growth was not fully determined. Is there something fundamental about the turbulence generated by this kind of shear that prevents field growth at all magnetic Reynolds numbers or is it just that e.g. the effective magnetic Reynolds number of the simulation had not reached the critical value for field growth? The difference between these two explanations is important because conventional wisdom from minimalist statistical methods of small scale magnetic field growth from turbulent flows at high enough Reynolds number would predict small scale dynamo action. We have revisited this issue with higher resolution simulations and our new preliminary results show that at higher resolution, Keplerian shear without the Coriolis force does in fact grow turbulent magnetic energy, even though lower resolution simulations do not. While pinning down the critical magnetic Reynolds number is still a work in progress for us (Nauman & Blackman in prep.), the result for simulations without explicit resistivity or viscosity is shown in Fig 4.

In addition, assessing whether large scale fields (i.e. fields for which the flux of suitably defined averages remains coherent over spatial or temporal scales that are large compared to those of fluctuations) are formed from *self-generated* linear shear driven turbulence is important in helping to identify the minimum conditions needed for large scale dynamos. Previous studies have found that *imposed* forcing of non-helical turbulence combined with linear shear leads to large scale field growth Yousef *et al.* (2008), possibly best interpreted as a "fluctuating" dynamo  $\alpha$  effect Heinemann *et al.* (2011).

5.2. *What are the non-local implications of shear periodic boundaries and absence of vertical differential rotation?*

Because the shear ( $y$ -velocity) in a shearing box has different signs at the inner and outer shear-periodic radial ( $x$ ) boundary while all other velocities and magnetic fields are periodic, quantities that depend on an odd power of the shear velocity such as the electric field, Poynting flux, and even the magnetic helicity flux (Hubbard & Brandenburg 2011; Hubbard *et al.* 2014) can be non-periodic. For the case with an initially radial mean field for example, an inflow of Poynting flux can non-locally add a comparable amount of energy to that supplied locally by the imposed shear (Hubbard *et al.* 2014). Even if there is no mean field across the box, fluctuations in velocity or magnetic that depend linearly on the background shear velocity are not guaranteed to be periodic.

What consequences do such fluxes have? The larger the boxes, the longer the timescales over which local dynamics in the box can be studied without the influence of the boundary term (Regev & Umurhan 2008), but the larger the boxes, the more unphysical it is to ignore curvature terms and vertical differential rotation (McNally & Pessah 2014) when interpreting the results for a real system.

5.3. *Are Shearing Boxes with Rotation and Very Large Reynolds Numbers Nonlinearly Stable?*

The question of whether rotating quasi-Keplerian shear flows can develop or sustain turbulence has lingered in both theoretical and laboratory contexts of Taylor-Couette flows (the latter being complicated by Ekman circulation) (Longaretti 2002; Lesur & Longaretti 2005; Paoletti & Lathrop 2011; Balbus 2011; Ji 2011; Schartman *et al.* 2012). We can however distinguish two sub-questions: (1) does the Coriolis force always stabilize an already turbulent flow? (2) does the Coriolis force prevent the onset of turbulence in the first place? If the answer to the first question were yes, then the answer to the second question would also likely be yes, but if the answer to the first question is no, then the answer to the second question would still be undetermined. While hydrodynamic modal analytic stability analyses and hydrodynamic shearing box simulations to date that include the Coriolis force have been found to be stable, there are physical reasons why instability may not yet be ruled out.

First, modal analysis is insufficient to prove the absence of nonlinear instability. The most relevant example is Couette flow, which is known to be linearly stable in a modal analysis, but unstable in the laboratory. Moreover, pseudospectral, non-modal methods also point to instability Trefethen *et al.* (1993). Second, because a linear shear flow without the Coriolis force is unstable, the question arises as to whether there is a range of scales, even in a rotating flow, where the influence of the Coriolis force on the flow is so weak that the flow appears to exhibit a purely linear shear with respect to nonlinear energy transfer. The time scale over which the Coriolis force acts on all scales is  $\Omega^{-1}$  where  $\Omega$  is the angular speed of the rotating frame, but a nonlinear cascade could proceed on a time scale  $\frac{l}{v(l)}$  where  $l$  is the eddy scale and  $v(l)$  is the velocity on that scale. This is particularly relevant to question (1) above: If nonlinear fluctuations or turbulence are already present, we might expect a dynamic range where the turnover times are much shorter than the rotation time. To capture this regime may require very high Reynolds numbers, but there could be a subset of the dynamic range above the dissipation range where the effect of the Coriolis force is small (Longaretti 2002).

A suggestive feature of the simulations in this context is that for the MRI unstable case, Fig 2 shows that the turbulence incurs a nonlinear cascade which is more anisotropic on large scales than small scales. As alluded to earlier, this suggests a nonlinear cascade

proceeding such that decreasing scales have relatively shortened nonlinear cascade time scales with respect to the shear time scale, which is independent of scale. In any case, the possibility that a subset of the dynamic range is less influenced by the Coriolis force cannot be identified from simple modal linear theory as evidenced by Eq. (4.3): The condition for stability  $K_A - T < 0$  is independent of scale in such a treatment.

#### 5.4. Vertical Stresses

Vertical stresses in shearing boxes are small compared to radial stresses and even negative (Miller & Stone 2000). For our run used to make Fig. 3 for example, we find the box averaged ratio of vertical Maxwell stress from fluctuations to radial Maxwell stress from fluctuations to be  $\frac{\langle v_y v_z \rangle - \langle b_y b_z \rangle}{\langle v_x v_y \rangle \langle b_x b_y \rangle} = -0.05$ . For real disks, it is unlikely that vertical stresses are negative. The prevalence of outflows, jets, and coronae suggest otherwise. The absence of vertical stratification in shearing boxes is a limitation (McNally & Pessah 2014) and global simulations will be an essential part of the enterprise to obtain realistic estimates of vertical stresses to inform mean field models.

## 6. Fundamental Challenges

### 6.1. Including Vertical and Non-local Transport in Mean Field Disc Models

As we have seen, the closure that produces the standard SS73 mean field model does not include non-local (large scale) radial stresses or any vertical stresses. Kuncic & Bicknell (2004, 2007) include mass loss and vertical angular momentum transport to an outflow using a mean field theory. However, they do not separately include vertical stresses from large and small scales as they do not include large scale magnetic fields. In computing the effect of the vertical transport on the observed radiation spectrum, they compute the reduction in disk emission rather than the specific spectral contributions of corona, jet, or wind.

Ultimately, we desire a dynamical theory that governs the relative contributions to transport from small scale and large scale magnetic fields and predicts the resultant spectral contributions of disk, corona and jet spectra. If the magnetic field is amplified in situ within the disc, then only structures large enough to overcome turbulent shredding Blackman & Pessah (2009) rise to coronae. The fraction can be determined if the magnetic energy and stress spectra in the disc can be determined. This provides a guiding principle towards quantifying the fraction of magnetic energy and stress that dissipate in coronae. Some relaxation of this coronal field to larger scales can provide global fields suitable for jets. Studying the processes by which large scale fields in accretion discs grow and evolve must be a component of this effort.

### 6.2. Role of Large scale dynamos in MRI simulations and Transport

In section 4 we discussed that transport emerging from the MRI is non-viscous and that large scale fluctuations and mean fields have a significant contribution to the stress. Large scale mean fields emerge in MRI unstable simulations with large enough vertical domains, whether stratified, unstratified, local or global. In shearing boxes or global disc simulations, vertically dependent mean fields are evident after averaging over radius ( $x$ ) and azimuth ( $y$ ), and exhibit cycle periods of  $\gtrsim 10$  orbits (Brandenburg *et al.* 1995; Lesur & Ogilvie 2010; Davis *et al.* 2010; Simon *et al.* 2011; Guan & Gammie 2011; Sorathia *et al.* 2012; Suzuki & Inutsuka 2014) (Shi *et al.* in prep.). In cylindrical global simulations with conducting walls, radially varying large scale fields are identified after vertically and azimuthally averaging (Ebrahimi & Bhattacharjee 2014). Understanding the mechanism

of the underlying large scale dynamo, the extent to which the stress spectra are converged, and the ratio of stress from mean fields to that from the total all need further work.

Whenever a large scale dynamo is present, a key unifying property is the presence of an electromotive force (per unit charge)  $\bar{\mathcal{E}} = \langle \mathbf{v} \times \mathbf{b} \rangle$ . The time evolution of the large scale field depends on the curl of the EMF. In mean field formalism, solving for the time evolution of the large scale field requires identifying a turbulent closure for the EMF in terms of the mean fields in the problem (namely, the mean magnetic field and mean velocities) analogous to the need to identify an appropriate closure for the stresses discussed in section 2. For weakly compressible flows, expansion of the EMF in terms of the mean field and its derivatives, reveals that large scale field growth is typically facilitated by a mean magnetic field aligned EMF such that  $\bar{\mathcal{E}} \cdot \bar{\mathbf{B}} \neq 0$ . The importance of  $\bar{\mathcal{E}} \cdot \bar{\mathbf{B}}$  also highlights the utility of tracking the temporal and spatial evolution of magnetic helicity (a topological measure of magnetic field line linkage) because  $\langle \bar{\mathcal{E}} \cdot \bar{\mathbf{B}} \rangle$  can be written as the sum of a time derivative of the magnetic helicity density associated with the large scale magnetic field plus a spatial divergence of large scale magnetic helicity flux plus a resistive term associated with the large scale current helicity. This same  $\bar{\mathcal{E}} \cdot \bar{\mathbf{B}}$  can also be written as the sum of a time derivative of mean small scale helicity density plus a spatial divergence of mean small scale magnetic helicity flux plus a resistive term associated with the mean small scale current helicity (see Brandenburg & Subramanian (2005); Blackman (2015) for reviews).

The connection between magnetic helicity and large scale astrophysical dynamos was first evident in the spectral model of helical MHD turbulence of Pouquet *et al.* (1976). They demonstrated an inverse transfer growth of large scale magnetic helicity for which the driver is the difference between kinetic and current helicities. Kleeorin & Ruzmaikin (1981) presented an equation that couples the small scale magnetic helicity to the mean electromotive force, but the time evolution was not studied. The spectral work of Pouquet *et al.* (1976) was re-derived as a time-dependent mean field theory without shear Blackman & Field (2002) and with shear Blackman & Brandenburg (2002)

The most important properties of magnetic helicity underlying its role in dynamo theory are: (1) For a given microphysical resistivity, the total magnetic helicity is better conserved than magnetic energy for typical MHD turbulent spectra (Blackman 2004). (2) For a given magnetic helicity, the energy of the field configuration is minimized when the magnetic field relaxes to the largest scale available subject to the boundary conditions. This can be approximately understood as follows: for a given wave number, magnetic energy in a helical field is  $\sim kH_M$  where  $H_M$  is the magnetic helicity, and so for fixed  $H_M$ , magnetic energy would decrease as  $k$  decreases. (3) Magnetic helicity can change rapidly on large scales and on small scales with opposite signs even when their sum total evolves only slowly on resistive time scales. (4) Magnetic helicity can flow through boundaries and can be exchanged spatially between sectors within a closed system.

During mean field growth, the field-aligned EMF is substantial but for a turbulent system in a saturated steady state, the growth terms and a turbulent decay terms may nearly cancel to a residual value that exactly compensates the microphysical resistive terms. When divergence terms are allowed (either by the global boundary conditions, or because the chosen averaging procedure involves retention of a subset of local spatial dependences), the EMF can be sustained by helicity fluxes. The importance of helicity fluxes to eject small scale magnetic helicity to maintain fast cycle periods and fast growth rates and avoid catastrophic quenching in stellar and galactic systems has been emphasized (Blackman & Field 2000*a,b*; Vishniac & Cho 2001; Vishniac 2009; Blackman & Brandenburg 2003; Brandenburg & Subramanian 2005; Shukurov *et al.* 2006; Ebrahimi & Bhattacharjee 2014) Recent observations of the sun (Zhang *et al.* 2012;

Pipin & Pevtsov 2014) suggest that both signs of helicity emerge in both hemispheres, a circumstance that helps resolve earlier concerns about which sign dominates Seehafer (1990) and the interpretation. When compared with simulations of large scale dynamos that use the same gauge as used to extract the vector potential from the observations (Pipin & Pevtsov 2014), the scale dependent signs of helicity measured from observations seem to agree with expected predictions (Blackman & Brandenburg 2003). That helicity flux can sustain or drive the growth of large scale fields in magnetically dominated fusion plasma relaxation or "laboratory plasma dynamos" has long been studied (Strauss 1985; Bhattacharjee & Hameiri 1986) and there are basic conceptual commonalities between laboratory and astrophysical dynamos despite the different plasma conditions.

The method of averaging can influence the specific form of terms contributing to  $\bar{\mathcal{E}}$  and its interpretation. The same system averaged in different ways might lead to different explanations of the differently computed mean magnetic fields (Blackman 2015). Mean fields in shearing boxes are typically computed as  $x, y$  planar averages leaving quantities as a function of  $z$  (see section 4), whereas mean fields in MRI simulations in global cylindrical systems with conducting boundaries have invoked azimuthal and vertical  $(\phi, z)$  averages (Ebrahimi & Bhattacharjee 2014).

Some have modeled the large scale cycle periods in shearing box simulations using traditional  $\alpha - \Omega$  type dynamos, with parameterized coefficients (Brandenburg & Donner 1997; Brandenburg 1998; Simon *et al.* 2011). Taking a step beyond this approach, Gressel (2010) identified that when the large scale field evolution is modeled by an  $\alpha - \Omega$  dynamo, the current helicity associated with fluctuations—as previously calculated for stratified sheared rotators Rüdiger & Kichatinov (1993)—seems to correlate well with the time-averaged behavior of  $\alpha$  empirically determined from the simulations. In addition, Gressel (2010) found that the time dependent dynamical quenching predicted using an  $\alpha$  effect represented by the difference between kinetic and current helicities is promising to explain the time dependent large scale dynamo. Others have begun to investigate in more detail the role and form of helicity fluxes in sustaining the EMF in MRI unstable flows ((Vishniac 2009; Käpylä & Korpi 2011; Ebrahimi & Bhattacharjee 2014; Squire & Bhattacharjee 2015*a,b*; Ebrahimi & Blackman in prep.) There is much to be done on this front, and to connect with the basic question of what minimal ingredients are needed for large scale dynamos, as alluded to above in section 5.1. Different circumstances, even if not minimal, likely lead to different important contributions to the EMF.

The presence and importance of large scale dynamos in accretion simulations is not entirely surprising because accretion disc theory and large scale dynamo theory are actually artificially separated components of what really should be captured by a unified mean field theory. Accretion disc theory has traditionally ignored the evolution of the large scale fields whilst mean field dynamo theory has ignored the dynamics of transport, and ultimately the two must operate together. There have been some steps along this path of unification (Rüdiger *et al.* 1993; Campbell & Caunt 1999; Campbell 2000; Moss *et al.* 2000; Rekowski *et al.* 2000; Moss & Shukurov 2004). These papers, along with Kuncic & Bicknell (2004) provide important starting points, but have not incorporated modern lessons learned from the MRI or magnetic helicity dynamics. Efforts to include all of these ingredients are beginning e.g Vishniac (2009); Ebrahimi & Bhattacharjee (2014) but we are far from the "practical model" stage in of predicting observed spectra and temporal evolution. Again there is much opportunity for further work.

### 6.3. Global Simulations and a Unified Mean Field Accretion/Dynamo Theory

Evidence for significant non-local transport by large scale fields is also evident in global simulations De Villiers & Hawley (2003); Fromang & Nelson (2006); Beckwith *et al.*

(2011); Sorathia *et al.* (2012); Penna *et al.* (2013); Suzuki & Inutsuka (2014). How the transport in such magnetized high magnetic Reynolds number discs proportions between disc, jets, outflows, and coronae and what determines this proportion is not yet understood.

A complicating feature is the interaction between disc and stellar or blackhole magnetosphere (Ghosh & Lamb 1978; Matt & Pudritz 2005; Küker *et al.* 2003; Perna *et al.* 2006; Romanova *et al.* 2012; Penna *et al.* 2012). If the spin of the central object such as a neutron star or black hole acts as a significant source of input energy, then the jet or coronae need not be entirely sourced by the accretion. The interaction undoubtedly influences jet formation, disc truncation, and the coronal energy supply, depending on the compactness, spin, and magnetic field of the central object.

There is evidence from numerical simulations Penna *et al.* (2013) that rapidly spinning black hole engines launch jets consistent with the mechanism of Blandford & Payne (1982) being dominant. And, as long as the simulations run long enough, emergence of the central jet appears to be independent of whether the initial field configuration consists of self-contained loops in the disc or more open initial large scale poloidal fields. The processes by which the field in the disc seeds the MRI, evolves and amplifies in the central regions (via some combination of advection and dynamo action), and subsequently relaxes to large scales to form jets all suggests that tracking magnetic helicity evolution will provide useful insight. Conceptually, a generic set of processes seems to be occurring: field amplification in a flow-dominated disc produces structures with large enough scale to buoyantly rise into the corona and avoid turbulent shredding. Once in the corona, some of these structures relax to form very large fields in the low plasma  $\beta$  regime corona. Generalizations of the simulations of Penna *et al.* (2013) to include a wider range of initial configurations with even smaller scale initial fields would be of interest.

If global simulations ultimately reveal that a diversity of initial states lead to a much less diverse set of end states, that is a helpful guide for mean field theories that couple accretion, field growth, coronae and jets. Some use of mean-field theory as an input to global simulations is emerging Stepanovs *et al.* (2014); Sądowski *et al.* (2015) but also important is the other direction-informing mean field models with outputs from global simulations. For most of the long history of simulations of jets (Pudritz *et al.* 2012), the magnetic fields have been imposed and the disc treated as a boundary condition but the new generation of simulations is evolving beyond this limitation. A similar evolution between connecting interior to exterior is emerging in solar dynamo simulations as well (Nelson *et al.* 2011; Nelson & Miesch 2014).

#### 6.4. Quantifying the precision of mean field models

In section 2 we explained that standard axisymmetric accretion theory makes sense only as a mean field theory and thus has a finite precision. In fact, both mean field dynamo and accretion theory are subject to the need to quantify this finite precision. There has been only limited work toward this goal Blackman (1998); Blackman *et al.* (2010). The precision of the theory itself depends on the size and temporal scales of the fluctuations over which averaging must take place to construct the mean field theory. The larger these fluctuations, the less precise the theory. There is a wide range of ratios of observational integration times vs. dynamical times in accreting systems, but characterization of this imprecision is particularly important when the integration times are very short such as for YSO infrared observations. Apparent disagreements between observations and theory must be evaluated with theoretical imprecision kept in mind. By analogy, offsets between the emergent spin axis and magnetic axis in stars or planets with dynamos need

not require a separate systematic physical explanation if such deviations are consistent simply with the predicted statistical imprecision in the mean field dynamo theory itself.

#### 6.5. *Developing an analogue to the H-R Diagram for Accretion Discs?*

If we are to ultimately understand disc evolution to a level that matches stellar evolution, we will need a characterization of observations analogous to that of the Hertzsprung-Russell diagram for stars. This should provide a systematic way to document the evolution of discs through various states of luminosity, coronal, and outflow activity. For accretion discs, the effective surface temperature varies outward across the surface of the disc, although the emission from the inner most regions likely dominates the luminosity. Among the features to capture in a diagram might be how far the thermal component of the disc extends inward, a measure of the fraction of non-thermal vs. thermal emission (spectral hardness), a measure of the jet contribution, and a characterization of variability. For a given type of accretion engine, the evolution through these states may depend primarily on the accretion rate. For microquasars, the long-observed evolution between states are being characterized by such diagrams Zhang (2013); Kylafis & Belloni (2015). Generalizing such diagrams to other types of accretion engines is important.

Black hole and stellar accreters have a range of masses whereas white dwarf and neutron star masses do not vary much. For rapidly spinning neutron stars, black holes, and classical novae, there are additional energy sources beyond that of the accretion itself. All such properties should be ultimately evident in the ensemble of evolutionary paths on appropriate state diagrams that provide the H-R diagram analogue.

## 7. Conclusions

While there has elsewhere been discussion of the small scale collisionless plasma frontier of accretion discs, here we have emphasized that incorporating large scale non-viscous transport into practical accretion disc models even for collisional systems is also a frontier. The need arises from observations of coronae and jets and from theory and simulations. We have discussed how standard SS73 accretion theory emerges from a statistical mean field theory and closure that does not include large scale transport and we have also discussed how even local shearing box simulations highlight the dominant contributions to transport stresses from large scale fluctuations and mean fields. These results emerge from analyses of the Maxwell stress spectra, the stress contributions from mean fields, analyses and interpretation of magnetic field tilt angles, and study of the extent to which observed stresses deviate in behavior from a simple viscosity. We have also emphasized the caveat that the stresses measured in shearing box simulations represent transporters of linear momenta (rather than angular momentum) therein and discussed how the standard physical interpretation of the MRI applies to a shearing box.

At present, spectral modelers typically use separate models for the thermal disc, coronae, and jets and patch them together in fraction needed to match observations. Instead, can a "first principles" mean field theory be developed to account for these fractions and their evolution self-consistently? The large scale magnetic fields that emerge in local and global MRI simulations also tell us that mean field accretion theory and mean field dynamo theory must be two faces of a single theory.

While global simulations represent the numerical frontier, the ultimate goal of understanding accretion discs at the level that stellar evolution is understood will not come from simulations alone. As the utility of SS73 has proven, a practical framework for use by modelers is invaluable for practical application and phenomenological interpretation. Overall, an important goal of future numerical work in combination with lessons



learned over the past  $\sim 20$  years should be to help inform a common-use generalization of SS73 that incorporates large scale transport self-consistently. In addition, a diagrammatic framework for accretion discs analogous to the H-R diagram (possibly of luminosity vs. spectral hardness) for all classes of accreters would be useful for efficiently classifying and organizing the observations.

Any mean field theory of a stochastic system, including that of SS73, has a finite statistical precision, and so the extent to which the theoretical predictions can be expected to accurately match a set of observations depends on making a careful correspondence between how the observed data are averaged compared to how the theory is averaged. If the observation times are short for example, large fluctuations could be misconstrued as differences between theory and observation. This issue is not widely recognized because it is often forgotten that practical accretion disc theory is formally a mean field theory with a specific choice of turbulent closure.

Finally, we note that computational limitations have in part contributed to often artificial separation of mutually intertwined processes in accretion engines: angular momentum transport, large scale dynamo action, corona formation, and jet formation. The recognition that all must part of a single theory has an analogue in solar physics. Coronal activity, flux transport dynamos, and convective interior dynamos are often studied separately because of the large dynamic range of scales needed to cover all of the processes involved. Often the latter two dynamo types are presented as distinct theories Charbonneau (2014). But ultimately any interior dynamo action must link to the corona to match the surface flux transport and observed solar cycle. Therefore, ingredients from all of these processes are also likely intertwined and simulations are beginning to capture this Nelson *et al.* (2011); Nelson & Miesch (2014).

Acknowledgements: E.B. acknowledges support from a Simons Foundation Fellowship and an IBM-Einstein Fellowship at IAS, and grants NSF-AST-1109285 and HST-AR-13916. F.N. acknowledges a Horton Graduate Fellowship for the Laboratory for Laser Energetics at U. Rochester. We thank A. Bhattacharjee, F. Ebrahimi, T. Heinemann, J. Owen, M. Pessah, Y. Shi, J. Squire, K. Subramanian, and I. Yi for related discussions.

#### REFERENCES

- ABRAMOWICZ, M., BRANDENBURG, A. & LASOTA, J.-P. 1996 The dependence of the viscosity in accretion discs on the shear/vorticity ratio. *MNRAS* **281**, L21–L24.
- ASADA, K., INOUE, M., NAKAMURA, M., KAMENO, S. & NAGAI, H. 2008 Multifrequency Polarimetry of the NRAO 140 Jet: Possible Detection of a Helical Magnetic Field and Constraints on Its Pitch Angle. *ApJ* **682**, 798–802.
- BALBUS, S. A. 2003 Enhanced Angular Momentum Transport in Accretion Disks. *ARAA* **41**, 555–597.
- BALBUS, S. A. 2011 Fluid dynamics: A turbulent matter. *Nature* **470**, 475–476.
- BALBUS, S. A. & HAWLEY, J. F. 1991 A powerful local shear instability in weakly magnetized disks. I - Linear analysis. II - Nonlinear evolution. *ApJ* **376**, 214–233.
- BALBUS, S. A. & HAWLEY, J. F. 1998 Instability, turbulence, and enhanced transport in accretion disks. *Reviews of Modern Physics* **70**, 1–53.
- BARRANCO, J. A. & MARCUS, P. S. 2005 Three-dimensional Vortices in Stratified Protoplanetary Disks. *ApJ* **623**, 1157–1170.
- BECKWITH, K., ARMITAGE, P. J. & SIMON, J. B. 2011 Turbulence in global simulations of magnetized thin accretion discs. *MNRAS* **416**, 361–382.
- BHATTACHARJEE, A. & HAMEIRI, E. 1986 Self-consistent dynamolike activity in turbulent plasmas. *Physical Review Letters* **57**, 206–209.
- BLACKMAN, E. G. 1998 Variability associated with alpha accretion disc theory for standard and advection-dominated discs. *MNRAS* **299**, L48–L52.

- BLACKMAN, E. G. 1999 On particle energization in accretion flows. *MNRAS* **302**, 723–730.
- BLACKMAN, E. G. 2004 How spectral shapes of magnetic energy and magnetic helicity influence their respective decay timescales. *Plasma Physics and Controlled Fusion* **46**, 423–430.
- BLACKMAN, E. G. 2015 Magnetic Helicity and Large Scale Magnetic Fields: A Primer. *Sp Sci. Rev.* **188**, 59–91.
- BLACKMAN, E. G. & BRANDENBURG, A. 2002 Dynamic Nonlinearity in Large-Scale Dynamos with Shear. *ApJ* **579**, 359–373.
- BLACKMAN, E. G. & BRANDENBURG, A. 2003 Doubly Helical Coronal Ejections from Dynamos and Their Role in Sustaining the Solar Cycle. *ApJL* **584**, L99–L102.
- BLACKMAN, E. G. & FIELD, G. B. 2000a Constraints on the Magnitude of  $\alpha$  in Dynamo Theory. *ApJ* **534**, 984–988.
- BLACKMAN, E. G. & FIELD, G. B. 2000b Coronal activity from dynamos in astrophysical rotators. *MNRAS* **318**, 724–732.
- BLACKMAN, E. G. & FIELD, G. B. 2002 New Dynamical Mean-Field Dynamo Theory and Closure Approach. *Physical Review Letters* **89** (26), 265007.
- BLACKMAN, E. G., FRANK, A. & WELCH, C. 2001 Magnetohydrodynamic Stellar and Disk Winds: Application to Planetary Nebulae. *ApJ* **546**, 288–298.
- BLACKMAN, E. G. & LUCCHINI, S. 2014 Using kinematic properties of pre-planetary nebulae to constrain engine paradigms. *MNRAS* **440**, L16–L20.
- BLACKMAN, E. G., NAUMAN, F. & EDGAR, R. G. 2010 Quantifying the Imprecision of Accretion Theory and Implications for Multi-Epoch Observations of Protoplanetary Discs. *ArXiv e-prints*.
- BLACKMAN, E. G., PENNA, R. F. & VARNIÈRE, P. 2008 Empirical relation between angular momentum transport and thermal-to-magnetic pressure ratio in shearing box simulations. *New Astronomy* **13**, 244–251.
- BLACKMAN, E. G. & PESSAH, M. E. 2009 Coronae as a Consequence of Large-Scale Magnetic Fields in Turbulent Accretion Disks. *ApJL* **704**, L113–L117.
- BLANDFORD, R. D. & BEGELMAN, M. C. 1999 On the fate of gas accreting at a low rate on to a black hole. *MNRAS* **303**, L1–L5.
- BLANDFORD, R. D. & PAYNE, D. G. 1982 Hydromagnetic flows from accretion discs and the production of radio jets. *MNRAS* **199**, 883–903.
- BODO, G., CATTANEO, F., MIGNONE, A. & ROSSI, P. 2014 On the Convergence of Magnetorotational Turbulence in Stratified Isothermal Shearing Boxes. *ApJL* **787**, L13.
- BONDI, H. 1952 On spherically symmetrical accretion. *MNRAS* **112**, 195.
- BRANDENBURG, A. 1998 Disc turbulence and viscosity. In *Theory of Black Hole Accretion Disks* (ed. M. A. Abramowicz, G. Björnsson & J. E. Pringle), pp. 61–90.
- BRANDENBURG, A. & DONNER, K. J. 1997 The dependence of the dynamo alpha on vorticity. *MNRAS* **288**, L29–L33.
- BRANDENBURG, A., NORDLUND, A., STEIN, R. F. & TORKESSON, U. 1995 Dynamo-generated Turbulence and Large-Scale Magnetic Fields in a Keplerian Shear Flow. *ApJ* **446**, 741.
- BRANDENBURG, A. & SUBRAMANIAN, K. 2005 Astrophysical magnetic fields and nonlinear dynamo theory. *Phys. Reports* **417**, 1–209.
- CALVET, N., D’ALESSIO, P., WATSON, D. M., FRANCO-HERNÁNDEZ, R., FURLAN, E., GREEN, J., SUTTER, P. M., FORREST, W. J., HARTMANN, L., UCHIDA, K. I., KELLER, L. D., SARGENT, B., NAJITA, J., HERTER, T. L., BARRY, D. J. & HALL, P. 2005 Disks in Transition in the Taurus Population: Spitzer IRS Spectra of GM Aurigae and DM Tauri. *ApJL* **630**, L185–L188.
- CAMPBELL, C. G. 2000 An accretion disc model with a magnetic wind and turbulent viscosity. *MNRAS* **317**, 501–527.
- CAMPBELL, C. G. 2003 A semi-analytic solution for the radial and vertical structure of accretion discs with a magnetic wind. *MNRAS* **345**, 123–143.
- CAMPBELL, C. G. & CAUNT, S. E. 1999 An analytic model for magneto-viscous accretion discs. *MNRAS* **306**, 122–136.
- CHARBONNEAU, P. 2014 Solar Dynamo Theory. *ARAA* **52**, 251–290.
- COLGATE, S. A., CEN, R., LI, H., CURRIER, N. & WARREN, M. S. 2003 Cosmological Mestel Disks and the Rossby Vortex Instability: The Origin of Supermassive Black Holes. *ApJL* **598**, L7–L10.

- DAVIS, S. W., STONE, J. M. & PESSAH, M. E. 2010 Sustained Magnetorotational Turbulence in Local Simulations of Stratified Disks with Zero Net Magnetic Flux. *ApJ* **713**, 52–65.
- DE VILLIERS, J.-P. & HAWLEY, J. F. 2003 Global General Relativistic Magnetohydrodynamic Simulations of Accretion Tori. *ApJ* **592**, 1060–1077.
- EBRAHIMI, F. & BHATTACHARJEE, A. 2014 Helicity-Flux-Driven  $\alpha$  Effect in Laboratory and Astrophysical Plasmas. *Physical Review Letters* **112** (12), 125003.
- FIELD, G. B. & ROGERS, R. D. 1993 Radiation from magnetized accretion disks in active galactic nuclei. *ApJ* **403**, 94–109.
- FLOCK, M., DZYURKEVICH, N., KLAHR, H., TURNER, N. & HENNING, T. 2012 Large-scale Azimuthal Structures of Turbulence in Accretion Disks: Dynamo Triggered Variability of Accretion. *ApJ* **744**, 144.
- FROMANG, S. 2010 MHD simulations of the magnetorotational instability in a shearing box with zero net flux: the case  $\text{Pm} = 4$ . *A&A* **514**, L5.
- FROMANG, S. & NELSON, R. P. 2006 Global MHD simulations of stratified and turbulent protoplanetary discs. I. Model properties. *A&A* **457**, 343–358.
- GABUZDA, D. C., CHRISTODOULOU, D. M., CONTOPOULOS, I. & KAZANAS, D. 2012 Evidence for Helical Magnetic fields in Kiloparsec-Scale AGN Jets and the Action of a Cosmic Battery. *Journal of Physics Conference Series* **355** (1), 012019.
- GAMMIE, C. F. 1996 Linear Theory of Magnetized, Viscous, Self-gravitating Gas Disks. *ApJ* **462**, 725.
- GAMMIE, C. F. & MENO, K. 1998 On the Origin of Episodic Accretion in Dwarf Novae. *ApJL* **492**, L75–L78.
- GHISELLINI, G., TAVECCHIO, F., MARASCHI, L., CELOTTI, A. & SBARRATO, T. 2014 The power of relativistic jets is larger than the luminosity of their accretion disks. *Nature* **515**, 376–378.
- GHOSH, P. & LAMB, F. K. 1978 Disk accretion by magnetic neutron stars. *ApJL* **223**, L83–L87.
- GIERLIŃSKI, M. & ZDZIARSKI, A. A. 1999 Accretion Disk in CYG X-1 in the Soft State. In *High Energy Processes in Accreting Black Holes* (ed. J. Poutanen & R. Svensson), *Astronomical Society of the Pacific Conference Series*, vol. 161, p. 64.
- GRESSEL, O. 2010 A mean-field approach to the propagation of field patterns in stratified magnetorotational turbulence. *MNRAS* **405**, 41–48.
- GUAN, X. & GAMMIE, C. F. 2011 Radially Extended, Stratified, Local Models of Isothermal Disks. *ApJ* **728**, 130.
- HARTNOLL, S. A. & BLACKMAN, E. G. 2000 Reprocessed emission from warped accretion discs with application to X-ray iron line profiles. *MNRAS* **317**, 880–892.
- HAWLEY, J. F., GAMMIE, C. F. & BALBUS, S. A. 1996 Local Three-dimensional Simulations of an Accretion Disk Hydromagnetic Dynamo. *ApJ* **464**, 690.
- HAWLEY, J. F., GUAN, X. & KROLIK, J. H. 2011 Assessing Quantitative Results in Accretion Simulations: From Local to Global. *ApJ* **738**, 84.
- HEINEMANN, T., MCWILLIAMS, J. C. & SCHEKOCHIHIN, A. A. 2011 Large-Scale Magnetic Field Generation by Randomly Forced Shearing Waves. *Physical Review Letters* **107** (25), 255004.
- HOYLE, F. & LYTTLETON, R. A. 1939 The evolution of the stars. *Proceedings of the Cambridge Philosophical Society* **35**, 592.
- HUBBARD, A. & BRANDENBURG, A. 2011 Magnetic Helicity Flux in the Presence of Shear. *ApJ* **727**, 11.
- HUBBARD, A., MCNALLY, C. P., OISHI, J. S., LYRA, W. & MAC LOW, M.-M. 2014 Radial Stresses and Energy Transport in Accretion Disks. *ArXiv e-prints*.
- JI, H. 2011 Current status and future prospects for laboratory study of angular momentum transport relevant to astrophysical disks. In *IAU Symposium* (ed. A. Bonanno, E. de Gouveia Dal Pino & A. G. Kosovichev), *IAU Symposium*, vol. 274, pp. 18–25. Cambridge Univ. Press.
- KANT, I. 1755 *Universal Natural History and Theory of the Heavens; Engl. translation (1968)*, in *W. Ley (ed.) Kants Cosmogony*. Greenwood Publishing (New York).
- KÄPYLÄ, P. J. & KORPI, M. J. 2011 Magnetorotational instability driven dynamos at low magnetic Prandtl numbers. *MNRAS* **413**, 901–907.
- KIM, K. H., WATSON, D. M., MANOJ, P., FORREST, W. J., NAJITA, J., FURLAN, E., SARGENT,

- B., ESPAILLAT, C., MUZEROLLE, J., MEGEATH, S. T., CALVET, N., GREEN, J. D. & ARNOLD, L. 2013 Transitional Disks and Their Origins: An Infrared Spectroscopic Survey of Orion A. *ApJ* **769**, 149.
- KING, A. R., PRINGLE, J. E. & LIVIO, M. 2007 Accretion disc viscosity: how big is alpha? *MNRAS* **376**, 1740–1746.
- KLAHR, H. H. & BODENHEIMER, P. 2003 Turbulence in Accretion Disks: Vorticity Generation and Angular Momentum Transport via the Global Baroclinic Instability. *ApJ* **582**, 869–892.
- KLEEORIN, N.I. & RUZMAIKIN, A. A. 1981 Dynamics of the mean turbulent helicity in magnetic field. Magnetohydrodynamics. *Magnetohydrodynamics* **18**, 116–122.
- KÖNIGL, A. 1989 Self-similar models of magnetized accretion disks. *ApJ* **342**, 208–223.
- KOTKO, I. & LASOTA, J.-P. 2012 The viscosity parameter  $\alpha$  and the properties of accretion disc outbursts in close binaries. *A&A* **545**, A115.
- KÜKER, M., HENNING, T. & RÜDIGER, G. 2003 Magnetic Star-Disk Coupling in Classical T Tauri Systems. *ApJ* **589**, 397–409.
- KUNCIC, Z. & BICKNELL, G. V. 2004 Dynamics and Energetics of Turbulent, Magnetized Disk Accretion around Black Holes: A First-Principles Approach to Disk-Corona-Outflow Coupling. *ApJ* **616**, 669–687.
- KUNCIC, Z. & BICKNELL, G. V. 2007 Towards a new standard model for black hole accretion. *Ap& Spac. Sup.* **311**, 127–135.
- KYLAFIS, N. D. & BELLONI, T. M. 2015 Accretion and Ejection in Black-Hole X-Ray Transients. In *Astrophysics and Space Science Library* (ed. I. Contopoulos, D. Gabuzda & N. Kylafis), *Astrophysics and Space Science Library*, vol. 414, p. 245. EDP Sciences.
- LAI, D. 2014 Theory of Disk Accretion onto Magnetic Stars. In *European Physical Journal Web of Conferences, European Physical Journal Web of Conferences*, vol. 64, p. 1001. EDP Sciences.
- LAPLACE, P. 1796 *Exposition du Sytme du Monde*, (Reprinted in the *Cambridge Library Collection; 2009*). Cambridge Univ. Press.
- LESUR, G. & LONGARETTI, P.-Y. 2005 On the relevance of subcritical hydrodynamic turbulence to accretion disk transport. *A&A* **444**, 25–44.
- LESUR, G. & OGILVIE, G. I. 2010 On the angular momentum transport due to vertical convection in accretion discs. *MNRAS* **404**, L64–L68.
- LI, H., FINN, J. M., LOVELACE, R. V. E. & COLGATE, S. A. 2000 Rossby Wave Instability of Thin Accretion Disks. II. Detailed Linear Theory. *ApJ* **533**, 1023–1034.
- LIH, P. S., ROMANOVA, M. M., USTYUGOVA, G. V., KOLDOBA, A. V. & LOVELACE, R. V. E. 2014 Propeller-driven outflows from an MRI disc. *MNRAS* **441**, 86–100.
- LONGARETTI, P.-Y. 2002 On the Phenomenology of Hydrodynamic Shear Turbulence. *ApJ* **576**, 587–598.
- LOVELACE, R. V. E., LI, H., COLGATE, S. A. & NELSON, A. F. 1999 Rossby Wave Instability of Keplerian Accretion Disks. *ApJ* **513**, 805–810.
- LYNDEN-BELL, D. 1969 Galactic Nuclei as Collapsed Old Quasars. *Nature* **223**, 690–694.
- LYNDEN-BELL, D. 2006 Magnetic jets from swirling discs. *MNRAS* **369**, 1167–1188.
- MATT, S. & PUDRITZ, R. E. 2005 The spin of accreting stars: dependence on magnetic coupling to the disc. *MNRAS* **356**, 167–182.
- MCNALLY, C. P. & PESSAH, M. E. 2014 On Vertically Global, Horizontally Local Models for Astrophysical Disks. *ArXiv e-prints* .
- MILLER, K. A. & STONE, J. M. 2000 The Formation and Structure of a Strongly Magnetized Corona above a Weakly Magnetized Accretion Disk. *ApJ* **534**, 398–419.
- MOSS, D. & SHUKUROV, A. 2004 Accretion disc dynamos opened up by external magnetic fields. *A&A* **413**, 403–414.
- MOSS, D., SHUKUROV, A. & SOKOLOFF, D. 2000 Accretion and galactic dynamos. *A&A* **358**, 1142–1150.
- MUSHOTZKY, R. F., DONE, C. & POUNDS, K. A. 1993 X-ray spectra and time variability of active galactic nuclei. *ARAA* **31**, 717–761.
- NAUMAN, F. & BLACKMAN, E. G. 2014 On characterizing non-locality and anisotropy for the magnetorotational instability. *MNRAS* **441**, 1855–1860.

- NAUMAN, F. & BLACKMAN, E. G. 2015 Sensitivity of the magnetorotational instability to the shear parameter in stratified simulations. *MNRAS* **446**, 2102–2109.
- NELSON, N. J., BROWN, B. P., BRUN, A. S., MIESCH, M. S. & TOOMRE, J. 2011 Buoyant Magnetic Loops in a Global Dynamo Simulation of a Young Sun. *ApJL* **739**, L38.
- NELSON, N. J. & MIESCH, M. S. 2014 Generating buoyant magnetic flux ropes in solar-like convective dynamos. *Plasma Physics and Controlled Fusion* **56** (6), 064004.
- OGILVIE, G. I. 2003 On the dynamics of magnetorotational turbulent stresses. *MNRAS* **340**, 969–982.
- PAOLETTI, M. S. & LATHROP, D. P. 2011 Angular Momentum Transport in Turbulent Flow between Independently Rotating Cylinders. *Physical Review Letters* **106** (2), 024501.
- PARKIN, E. R. & BICKNELL, G. V. 2013 Global simulations of magnetorotational turbulence - I. Convergence and the quasi-steady state. *MNRAS* **435**, 2281–2298.
- PENNA, R. F., NARAYAN, R. & SĄDOWSKI, A. 2013 General relativistic magnetohydrodynamic simulations of Blandford-Znajek jets and the membrane paradigm. *MNRAS* **436**, 3741–3758.
- PENNA, R. F., SĄDOWSKI, A. & MCKINNEY, J. C. 2012 Thin-disc theory with a non-zero-torque boundary condition and comparisons with simulations. *MNRAS* **420**, 684–698.
- PÉREZ, L. M., ISELLA, A., CARPENTER, J. M. & CHANDLER, C. J. 2014 Large-scale Asymmetries in the Transitional Disks of SAO 206462 and SR 21. *ApJL* **783**, L13.
- PERNA, R., BOZZO, E. & STELLA, L. 2006 On the Spin-up/Spin-down Transitions in Accreting X-Ray Binaries. *ApJ* **639**, 363–376.
- PESSAH, M. E., CHAN, C.-K. & PSALTIS, D. 2006 Local Model for Angular-Momentum Transport in Accretion Disks Driven by the Magnetorotational Instability. *Physical Review Letters* **97** (22), 221103.
- PESSAH, M. E., CHAN, C.-K. & PSALTIS, D. 2007 Angular Momentum Transport in Accretion Disks: Scaling Laws in MRI-driven Turbulence. *ApJL* **668**, L51–L54.
- PESSAH, M. E., CHAN, C.-K. & PSALTIS, D. 2008 The fundamental difference between shear alpha viscosity and turbulent magnetorotational stresses. *MNRAS* **383**, 683–690.
- PIPIN, V. V. & PEVTSOV, A. A. 2014 Magnetic Helicity of the Global Field in Solar Cycles 23 and 24. *ApJ* **789**, 21.
- POUQUET, A., FRISCH, U. & LEORAT, J. 1976 Strong MHD helical turbulence and the nonlinear dynamo effect. *Journal of Fluid Mechanics* **77**, 321–354.
- PRENDERGAST, K. H. & BURBIDGE, G. R. 1968 On the Nature of Some Galactic X-Ray Sources. *ApJL* **151**, L83.
- PUDRITZ, R. E., HARDCASTLE, M. J. & GABUZDA, D. C. 2012 Magnetic Fields in Astrophysical Jets: From Launch to Termination. *Sp Sci. Rev.* **169**, 27–72.
- QUATAERT, E., HEINEMANN, T. & SPITKOVSKY, A. 2014 Linear Instabilities Driven by Differential Rotation in Very Weakly Magnetized Plasmas. *ArXiv e-prints*.
- QUATAERT, E. & NARAYAN, R. 1999 Spectral Models of Advection-dominated Accretion Flows with Winds. *ApJ* **520**, 298–315.
- REGEV, O. & UMURHAN, O. M. 2008 On the viability of the shearing box approximation for numerical studies of MHD turbulence in accretion disks. *A&A* **481**, 21–32.
- REKOWSKI, M. V., RÜDIGER, G. & ELSTNER, D. 2000 Structure and magnetic configurations of accretion disk-dynamo models. *A&A* **353**, 813–822.
- REYNOLDS, C. S. 2014 Measuring Black Hole Spin Using X-Ray Reflection Spectroscopy. *Sp Sci. Rev.* **183**, 277–294.
- RISALITI, G., HARRISON, F. A., MADSEN, K. K., WALTON, D. J., BOGGS, S. E., CHRISTENSEN, F. E., CRAIG, W. W., GREFFENSTETTE, B. W., HAILEY, C. J., NARDINI, E., STERN, D. & ZHANG, W. W. 2013 A rapidly spinning supermassive black hole at the centre of NGC 1365. *Nature* **494**, 449–451.
- ROMANOVA, M. M., USTYUGOVA, G. V., KOLDOBA, A. V. & LOVELACE, R. V. E. 2012 MRI-driven accretion on to magnetized stars: global 3D MHD simulations of magnetospheric and boundary layer regimes. *MNRAS* **421**, 63–77.
- RÜDIGER, G. 1987 Turbulence Theory and the Frictional Energy Source in Accretion Disk Models. *Acta Astr.* **37**, 223.
- RÜDIGER, G., ELSTNER, D. & SCHULTZ, M. 1993 Dynamo-driven accretion in galaxies. *A&A* **270**, 53–59.

- RÜDIGER, G. & KICHATINOV, L. L. 1993 Alpha-effect and alpha-quenching. *A&A* **269**, 581–588.
- SALPETER, E. E. 1964 Accretion of Interstellar Matter by Massive Objects. *ApJ* **140**, 796–800.
- SĄDOWSKI, A., NARAYAN, R., TCHEKHOVSKOY, A., ABARCA, D., ZHU, Y. & MCKINNEY, J. C. 2015 Global simulations of axisymmetric radiative black hole accretion discs in general relativity with a mean-field magnetic dynamo. *MNRAS* **447**, 49–71.
- SCHARTMAN, E., JI, H., BURIN, M. J. & GOODMAN, J. 2012 Stability of quasi-Keplerian shear flow in a laboratory experiment. *A&A* **543**, A94.
- SEEHAFER, N. 1990 Electric current helicity in the solar atmosphere. *Solar Phys.* **125**, 219–232.
- SHAKURA, N. I. & POSTNOV, K. A. 2014 On properties of Velikhov-Chandrasekhar MRI in ideal and non-ideal plasma. *ArXiv e-prints* .
- SHAKURA, N. I. & SUNYAEV, R. A. 1973 Black holes in binary systems. Observational appearance. *A&A* **24**, 337–355.
- SHKLOVSKII, I. S. 1963 On the Nature of Radio Galaxies. *Sov. Astron.* **6**, 465.
- SHUKUROV, A., SOKOLOFF, D., SUBRAMANIAN, K. & BRANDENBURG, A. 2006 Galactic dynamo and helicity losses through fountain flow. *A&A* **448**, L33–L36.
- SIMON, J. B., HAWLEY, J. F. & BECKWITH, K. 2011 Resistivity-driven State Changes in Vertically Stratified Accretion Disks. *ApJ* **730**, 94.
- SORATHIA, K. A., REYNOLDS, C. S., STONE, J. M. & BECKWITH, K. 2012 Global Simulations of Accretion Disks. I. Convergence and Comparisons with Local Models. *ApJ* **749**, 189.
- SQUIRE, J. & BHATTACHARJEE, A. 2015a Coherent nonhelical shear dynamos driven by magnetic fluctuations at low Reynolds numbers. *ArXiv e-prints* .
- SQUIRE, J. & BHATTACHARJEE, A. 2015b Electromotive force due to magnetohydrodynamic fluctuations in sheared rotating turbulence. *ArXiv e-prints* .
- STAPELFELDT, K. R., DUCHÊNE, G., PERRIN, M., WOLFF, S., KRIST, J. E., PADGETT, D. L., MÉNARD, F. & PINTE, C. 2014 HST Imaging of New Edge-on Circumstellar Disks in Nearby Star-forming Regions. In *IAU Symposium* (ed. M. Booth, B. C. Matthews & J. R. Graham), *IAU Symposium*, vol. 299, pp. 99–103. Cambridge Univ. Press.
- STEPANOV, D., FENDT, C. & SHEIKHNEZAMI, S. 2014 Modeling MHD Accretion-Ejection: Episodic Ejections of Jets Triggered by a Mean-field Disk Dynamo. *ApJ* **796**, 29.
- STRAUSS, H. R. 1985 The dynamo effect in fusion plasmas. *Physics of Fluids* **28**, 2786–2792.
- SUZUKI, T. K. & INUTSUKA, S.-I. 2014 Magnetohydrodynamic Simulations of Global Accretion Disks with Vertical Magnetic Fields. *ApJ* **784**, 121.
- SWEDENBORG, E. 1734 (*Principia*) *Latin: Opera Philosophica et Mineralia (English: Philosophical and Mineralogical Works) I.*
- TAGGER, M. & PELLAT, R. 1999 An accretion-ejection instability in magnetized disks. *A&A* **349**, 1003–1016.
- TAYLOR, G. B. & PERLEY, R. A. 1993 Magnetic Fields in the Hydra A Cluster. *ApJ* **416**, 554.
- TREFETHEN, L. N., TREFETHEN, A. E., REDDY, S. C. & DRISCOLL, T. A. 1993 Hydrodynamic stability without eigenvalues. *Science* **261**, 578–584.
- TREMAINE, S. & DAVIS, S. W. 2014 Dynamics of warped accretion discs. *MNRAS* **441**, 1408–1434.
- VAN DER MAREL, N., VAN DISHOCK, E. F., BRUDERER, S., BIRNSTIEL, T., PINILLA, P., DULLEMOND, C. P., VAN KEMPEN, T. A., SCHMALZL, M., BROWN, J. M., HERCZEG, G. J., MATHEWS, G. S. & GEERS, V. 2013 A Major Asymmetric Dust Trap in a Transition Disk. *Science* **340**, 1199–1202.
- VAN ECK, C. L., BROWN, J. C., SHUKUROV, A. & FLETCHER, A. 2015 Magnetic Fields in a Sample of Nearby Spiral Galaxies. *ApJ* **799**, 35.
- VARNIÈRE, P. & TAGGER, M. 2002 Accretion-Ejection Instability in magnetized disks: Feeding the corona with Alfvén waves. *A&A* **394**, 329–338.
- VELIKHOV, E. P. 1959 Stability of an Ideally Conducting Liquid Flowing Between Cylinders Rotating in a Magnetic Field. *Soviet Journal of Experimental and Theoretical Physics* **36**, 1398–1404.
- VISHNIAC, E. T. 2009 The Saturation Limit of the Magnetorotational Instability. *ApJ* **696**, 1021–1028.
- VISHNIAC, E. T. & CHO, J. 2001 Magnetic Helicity Conservation and Astrophysical Dynamos. *ApJ* **550**, 752–760.

- VOROBYOV, E. I. & BASU, S. 2007 Self-regulated gravitational accretion in protostellar discs. *MNRAS* **381**, 1009–1017.
- YOUSEF, T. A., HEINEMANN, T., SCHEKOCIHIN, A. A., KLEORIN, N., ROGACHEVSKII, I., ISKAKOV, A. B., COWLEY, S. C. & MCWILLIAMS, J. C. 2008 Generation of Magnetic Field by Combined Action of Turbulence and Shear. *Physical Review Letters* **100** (18), 184501.
- YUAN, F. & NARAYAN, R. 2014 Hot Accretion Flows Around Black Holes. *ARAAS* **52**, 529–588.
- ZEL'DOVICH, Y. B. 1964 The Fate of a Star and the Evolution of Gravitational Energy Upon Accretion. *Soviet Physics Doklady* **9**, 195.
- ZHANG, H., MOSS, D., KLEORIN, N., KUZANYAN, K., ROGACHEVSKII, I., SOKOLOFF, D., GAO, Y. & XU, H. 2012 Current Helicity of Active Regions as a Tracer of Large-scale Solar Magnetic Helicity. *ApJ* **751**, 47.
- ZHANG, S.-N. 2013 Black hole binaries and microquasars. *Frontiers of Physics* **8**, 630–660.
- ZHU, Z., HARTMANN, L., GAMMIE, C. & MCKINNEY, J. C. 2009 Two-dimensional Simulations of FU Orionis Disk Outbursts. *ApJ* **701**, 620–634.